Controlling Factors of Flow Separation in Natural, Meandering Streams

by

Irene Mulder

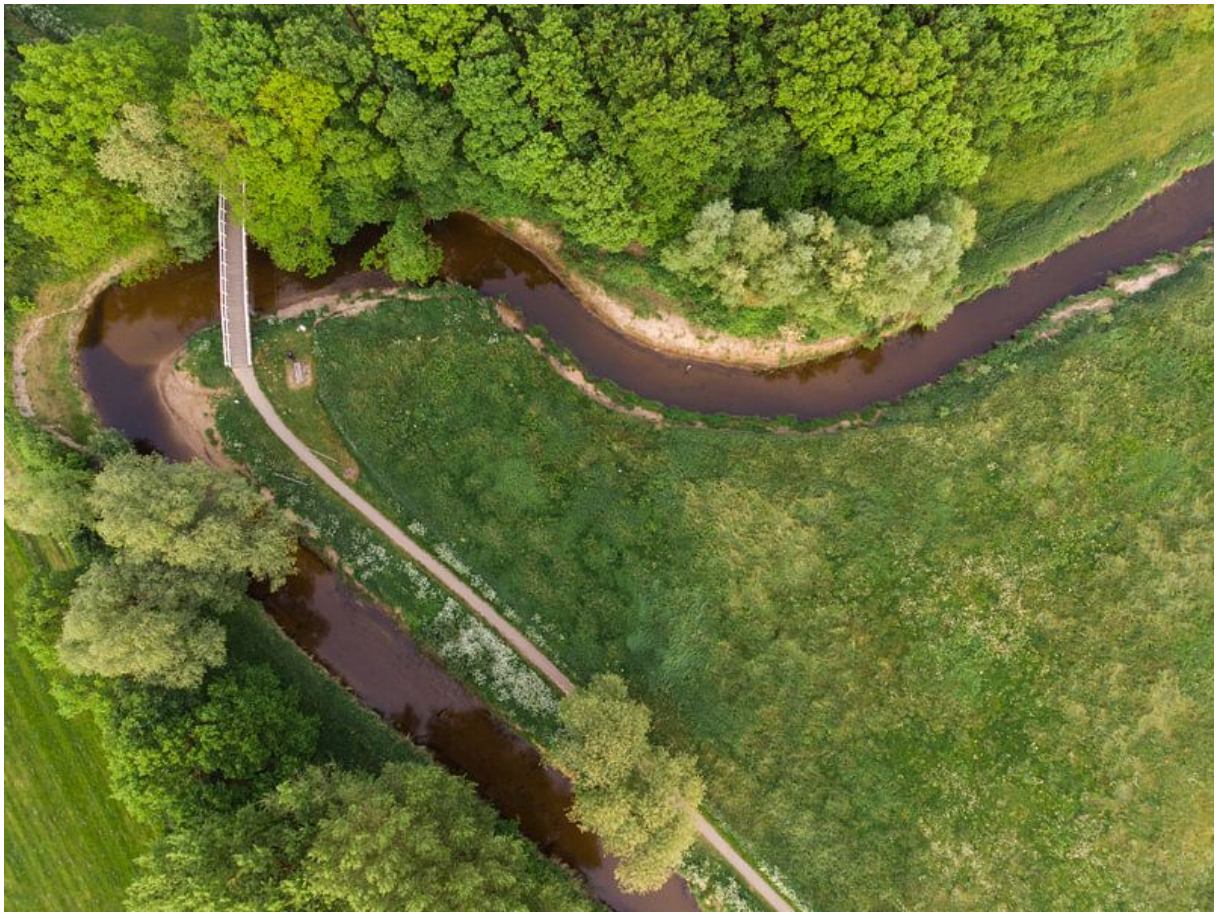

July 1, 2024

UNIVERSITY
OF TWENTE.

Controlling Factors of Flow Separation in Natural, Meandering Streams

by

Irene Mulder

Student number:
s2200201

to obtain the degree of Master of Science
at the University of Twente,
to be defended pubilcly on 09-07-2024

Photograph on the front page by Hasenbos (n.d.)

Head of Committee	dr. ir. D.C.M. (Denie) Augustijn
Daily Supervisor	dr. V (Vasileios) Kitsikoudis

UNIVERSITY
OF TWENTE.

Summary

Flow separation is a physical phenomenon that is observed near the banks of many meandering rivers. In these flow separation zones, the flow is either recirculating or stagnant and can occur both at the boundary of the inner and the boundary of the outer bend of rivers. These flow separation zones influence the hydraulics, ecology and morphodynamics of rivers, for example, by decreasing the effective width of the rivers and reducing their conveyance capacity. However, the exact conditions under which flow separation occurs and the extent to which they influence the size of the flow separation zones remain unclear.

Therefore, this study aims to answer the question:

Which geometric and flow characteristics are controlling factors for the onset and size of flow separation in the Glanerbeek?

This is done by executing field research at ten bends in the Glanerbeek, which is a stream in the region of Twente in the Netherlands. The field research was executed on three days. The aim of the field research is to obtain surface flow velocity patterns and cross-sectional profiles at various locations throughout the bend. The cross-sectional profiles are made with real-time kinematic positioning (RTK). The former surface flow velocity patterns are made with a Large Scale Particle Image Velocimetry (LSPIV) analysis, where tracers that are present at the surface of the flow are traced by a camera. In this case, the camera is mounted on a drone and a net is spanned across the stream to create natural tracers on the surface.
First, the influence of the distance from the reference location and the net, which generates the tracers, was studied. It was found that there is no direct relation between the distance from the net and the error. The amount of error appeared to be more location-specific than to be dependent on the distance from the net. A possible cause for these location-specific values of error can be the velocity at the reference location, as a positive correlation was found between the velocities and the accuracy.

Next, the optimal settings for the LSPIV analysis were researched. Three parameters were tested specifically: the sampling frequency, video length and interrogation area. The sampling frequency and interrogation area had a relatively large influence on the accuracy of the LSPIV analysis. The influence of the video length was rather small.

After that, the flow patterns calculated for each bend were analysed. It was found that inner bend separations were more apparent than outer bend separation zones and that the average size of the inner bend separation zones is a bit larger than the average size of the outer bend separation zones. The maximum flow velocity was higher during the first measurement day, as was the flow depth. Topographic steering was often observed and was stronger on the third measurement day. No inner bend recirculation zones were found, even though this was expected due to the presence of a point bar in the bends.

During the study, there was a specific focus on the following, potential, controlling factors:

- Flow depth
- Radius of the bend
- R/B ratio
- Impingement angle
- Increase in cross-sectional area

A correlation was found with all of these potential controlling factors. The strongest correlation was the increase in cross-sectional area with the outer bend separation zones, which showed that an increase in cross-sectional area leads to a decrease in the size of the outer bend separation zones. This is contrary to literature and could be caused by the methods used in this study. The impingement angle also showed a negative correlation with the outer bend separation zones, as did the radius of the river bend. The R/B ratio was the only parameter showing correlation with the inner bend separation zones, even though this correlation was stronger during the first measurement day. These correlating parameters could be controlling parameters for the onset of flow separation. However, no specific threshold values have been found that induce the onset of flow separation zones.

Contents

List of Tables

List of Figures

List of Symbols

Symbol	Description	Unit
A	cross-sectional area	m^2
B	width of the river	m
C_f	bottom friction coefficient	-
d	discrepancy between computed and reference velocities	%
D_*	dispersion index	-
Fr	Froude number	-
g	gravitational acceleration	$\mathrm{m\,s}^{-2}$
h	flow depth	m
Kr	advection-friction coefficient	-
L	centerline length of the river bend	m
n	number of reference velocities	-
n'	transverse coordinate	m
P	pressure	Pa
R	radius	m
r	Pearson correlation coefficient	-
ρ	density	$\mathrm{kg\,m}^{-3}$
ρ_{cv}	reference seeding density	ppp
ρ_s	seeding density	ppp
R_{min}	lowest value of the radius within a bend	m
s	distance in the longitudinal direction of the river bend	m
σ	standard deviation	
U_{ECM}	velocity measured by the ECM	$\mathrm{m\,s}^{-1}$
U_c	computed velocity by LSPIV	
U_r	reference velocity measured with the float method	$\mathrm{m\,s}^{-1}$
v	velocity	$\mathrm{m\,s}^{-1}$

1 Introduction

In many meandering rivers, flow separation zones are observed. These are zones where the boundary layer flow is separated from the channel banks and in which the velocity is close to zero or the flow is recirculating. These zones can occur both at the inner and the outer bend. The flow separation zones are displayed in Figure 1, as F6 and F7. Flow separation results in a reduction of the effective channel width (Parsons, 2003), which results in a reduced conveyance capacity (Blanckaert, 2015; Kleinhans et al., 2010). Moreover, flow separation can significantly increase the drag in a river, because of the pressure drop near the separation zone, which acts as an extra form drag (Bo and Ralston, 2020). Hence, it is important to study flow separation because it alters the flow pattern, which causes the migration and sedimentation patterns to differ from flows without flow separation (Ferguson et al., 2003). For example, outer bank separation zones protect the outer bank from erosion, while favoring deposition and growth of the point bar at the inner bank (Parsons, 2003). Moreover, Ferguson et al. (2003) found that the ecology within the flow separation zones differs from the main flow. In addition, flow separation reduces mixing of, for example, pollutants (Ferguson et al., 2003) and is known to be a source of anomalous transport in rivers, as the recirculation zones trap small particles that are present in the flow (Kim et al., 2020), such as suspended sediment particles and plant seedings (Merritt and Wohl, 2002).

In this study, the flow separation patterns within the Glanerbeek will be studied. This will be done with the use of Large Scale Particle Image Velocimetry (LSPIV), which is a non-invasive method for measuring the velocity at the surface of a flow. LSPIV has been used to study the flow pattern in different rivers, such as vegetated rivers (Creëlle et al., 2018), at river confluences (Lewis and Rhoads, 2018), and to study flash floods in mountain streams (Dramais et al., 2011; Ran et al., 2016). The tracers used are often artificial tracers (e.g. Bradley et al., 2002; Creëlle et al., 2018; Pearce et al., 2020) or natural tracers already present in the stream, for example, created by turbulence (Sharif, 2022) or suspended sediment (Legleiter and Kinzel, 2020).

Figure 2 displays the terminology that will be used in this study for the characteristics that are present in the river bends. If the characteristics are not described in this figure, they will be explained within the sections. Some terms that are often used are the apex, which denotes the vertex of the river bend, the pool, which is a deeper part of the river bend on the side of the outer bend and the point bar, which indicates the sediment present at the inner bend.

Flow separation can be found at the inner bend and at the outer bend of a river. Flow separation is caused by an adverse pressure gradient in the direction of the flow, which is caused by an imbalance of inertia, the centrifugal force and the centripetal force. Inertia moves the flow forward, creating an accumulation of mass at the outer bend, where the main flow is directed to (Blanckaert, 2015; Nanson, 2010). Due to this accumulation of mass, transverse tilting of the water surface occurs and thus a higher pressure near the outer bend (Vermeulen et al., 2015). Inner bend separation occurs downstream of the apex due to the transverse tilting of the water surface, while the outer bend separation occurs upstream of the apex (Hodskinson and Ferguson, 1998). For inner bend separation, the flow is already slowed down throughout the bend, making flow separation more likely to occur in the inner bend than the outer bend (Blanckaert, 2015; Parsons, 2003). The amount of transverse tilting can be approximated with the curvature, as it increases with increasing curvature (Blanckaert, 2010; Furbish, 1991). This increase in pressure can also be explained with the Bernoulli equation (Fox et al., 2016):

$$\frac{P}{\rho} + \frac{v^2}{2} + gh = constant \tag{1}$$

Where P is the pressure, ρ the density of the water, v the velocity, g the gravitational acceleration and h the water depth. Assuming incompressible flow, the pressure is dependent on the velocity and the water depth of the flow. Due to the transverse tilting at the outer bed, the water depth increases in the direction of the flow, but the velocity is simultaneously reduced, causing an increase in pressure and thus an adverse pressure gradient. The accumulation of the mass at the outer bend also causes an inward pressure gradient that causes the direction of the flow to change inward. However, this inward pressure gradient is delayed compared to the outward inertial forces, called the spatial lag. The inertial force can be described by the Froude number:

$$Fr = \frac{v}{\sqrt{gh}} \tag{2}$$

Where Fr is the velocity of the flow. Since g is a constant, the Froude number increases for higher velocities and lower water depths. Thus, the inertial forces are higher at high velocities and shallow streams.

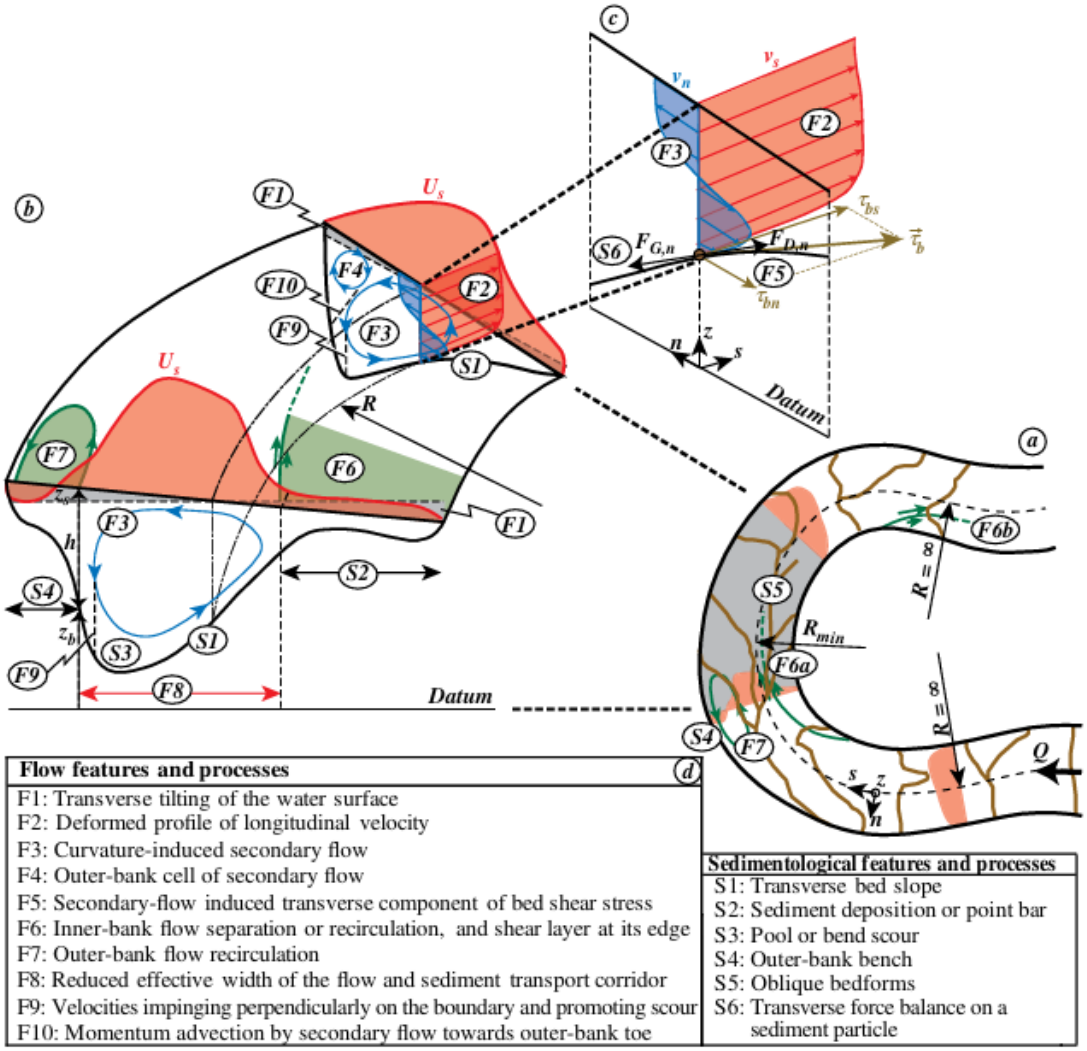

Figure 1: Schematic overview of the flow and sediment processes present in river bends where a) displays a planview of a river bend and b) displays a section of the river bend in a 3D - view. c) displays the velocity profile within the stream and d) describes the flow and sedimentological features and processes that are visible in a), b) and c) (Blanckaert, 2018)

The inward pressure gradient forces the flow away from the path of inertia. It scales with the ratio between the width (B) and the radius of the bend (R) (Blanckaert, 2015), meaning it is enhanced at larger R/B ratios. Lastly, the spatial lag between these forces is important because this creates the imbalance between the inertial forces and the inward and outward forces. The spatial lag is dependent on the change in curvature over space, defined by $\frac{\Delta R}{\Delta s}$, where s denotes the distance in the longitudinal direction of the bend (Blanckaert, 2015). Hence, if there is a sudden increase in curvature, the spatial lag is larger. Another factor influencing the spatial lag is the shallowness of the river, defined by the ratio B/h (Blanckaert, 2015). In shallow and wide rivers, the formation of the inward pressure gradient requires a longer distance than in deep and narrow rivers (Blanckaert, 2018), thus the spatial lag increases for shallow and wide rivers and favours flow separation.

While an adverse pressure gradient is a necessary condition for flow separation, it does not necessarily result in flow separation (Blanckaert, 2010). The free stream flow in the boundary layer at the banks is driven by horizontal velocity shear. A high shear at the banks, results in a thin boundary layer with a relatively high velocity gradient. As a result, the flow near the boundary is relatively strong, making separation of the flow more difficult (Vermeulen et al., 2015). Hence, the adverse pressure gradient needs to be large enough, with respect to the boundary layer, to direct the flow into the upstream direction. Conversely, at a bank with low shear, there is a thicker boundary layer with a less steep velocity gradient, which results in weaker flow near the boundary and easier flow separation. Bo and Ralston (2020) identified the advection-friction ratio Kr, which describes the relation between the friction and the advection within the river. Kr can be identified as:

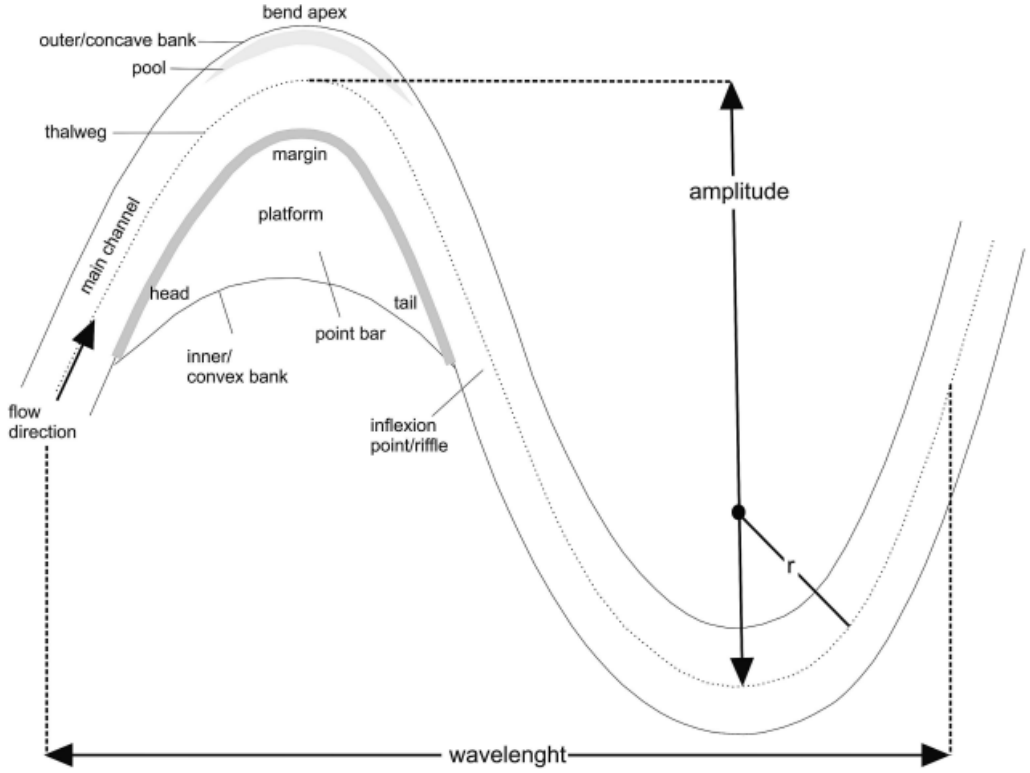

Figure 2: Illustration of the terminology used for river bends (Kasvi, 2015)

$$K_r = \frac{h}{C_f L} F(\frac{R}{B}) \tag{3}$$

Where C_f the bottom fiction coefficient, L the centerline length of the river bend and F denotes a function such that K_r increases with a decrease in the R/B ratio. R_{min} is the smallest centerline radius, which is the point of highest curvature calculated from the centerline of the river bend, as the curvature is calculated by $\frac{1}{R}$.

For K_r = 1, the advection equals the friction. For K_r < 1, friction is stronger than the advection which is opposed and when K_r > 1, the advection is stronger than the friction which is favorable for flow separation. While C_f is also dependent on the water depth, the influence of the water depth is larger on $\frac{h}{L}$ than on C_f (Bo and Ralston, 2020). Hence, this equation demonstrates that for an increase in $\frac{h}{L}$ and/or a decrease in $\frac{R}{B}$, K_r increases and flow separation is more apparent.

The relation between flow separation and $\frac{R}{B}$ in a river was also found by Bagnold (1960), who identified two stages of flow separation. The first stage of flow separation results in a stagnant separation zone, where the mean velocity in the separation zone is zero and the flow is stable. This occurs when R/B < 3. The second stage is characterized by unstable flow, with eddies and flow recirculation and emerges when R/B < 2 (Bagnold, 1960). The curvature and the ratio between the curvature and the width of the river are important factors in the onset of flow separation zones.

Flow separation can also be caused by an increase in cross-sectional area, which enhances the adverse pressure gradient (Vermeulen et al., 2015). This was found in a field study at a bend with a deep scour hole in the Mahakam river and the significance of the increase in cross-sectional area on flow separation was also found in canyons (Venditti et al., 2014). An increase in cross-sectional area is usually found with increasing bend curvature up until very sharp bends, where the increase in cross-sectional area stagnates (Vermeulen et al., 2015). No specific value for the stagnation of increase in cross-sectional area is known. However, the increase in cross-sectional area enhances the adverse water surface gradient. Vermeulen et al. (2015) developed the following equation for describing the adverse water surface gradient:

$$\frac{\Delta z}{\Delta s} = -C_f Fr^2 + Fr^2 \frac{\Delta}{\Delta s}(\frac{h}{R})n + \frac{Fr^2}{B}\frac{\Delta A}{\Delta s} \tag{4}$$

This equation is based on an earlier equation of Blanckaert et al. (2013), which is a combination of the depth-averaged transverse momentum equation and the streamwise water surface gradient. The third term on the right side is added by Vermeulen et al. (2015) to represent the change in cross-sectional area. In Equation 4, n' denotes the transverse coordinate and A the cross-sectional area of the bend. Thus, an increase in $\frac{\Delta A}{\Delta s}$ increases $\frac{\Delta z}{\Delta s}$. For an adverse water surface gradient:

$$\frac{\Delta z}{\Delta s} > 0 \tag{5}$$

$$-C_f Fr^2 + Fr^2 \frac{\Delta}{\Delta s}(\frac{h}{R})n + \frac{Fr^2}{B}\frac{\Delta A}{\Delta s} > 0 \tag{6}$$

Since n denotes the transverse coordinate, the second term will result in an adverse water surface gradient at the outer bend, and a favorable water surface gradient at the inner bend, due to the transverse tilting of the water surface.

Flow separation can also be observed in combination with topographic steering. Topographic steering is a process that directs the flow toward the outer bank and away from the point bar. The flow over the point bar is shallow, which causes an increase in pressure due to shoaling over the point bar and a decrease in pressure at the pool. This creates an outward directed flow that is stronger than the earlier mentioned adverse pressure caused by the accumulation of mass in the outer bend. As a result, the flow is directed towards the pool and flows around the point bar (Blanckaert, 2010). The high velocity field has often been observed to be located over the pool in the outer bend (Blanckaert, 2010; Ferguson et al., 2003; Nanson, 2010; Vermeulen et al., 2015). The direction of the flow over the pool is stronger for bends which are wide and shallow at the entry of the bend (Nanson, 2010). When the point bar is submerged, there is often flow recirculation over the point bar. This is also caused by an adverse water surface gradient, but is considerably weaker compared to the flow separation caused by the accumulation of mass (Blanckaert, 2010). Shallow flow over a bar is seen as one of the main formative conditions for the onset of inner bend recirculation zones (Blanckaert et al., 2013).

Due to topographic steering, the flow collides with the outer bank. After this collision, there is a rise in water surface elevation, causing downwelling of the flow. Due to this downwelling, the flow impinges on the bed and creates scour (Blanckaert, 2010). Due to transverse movement inward caused by secondary flow in the river bend, there is deposition on the point bar. This creates a positive feedback loop. The deposition on the point bar causes more pronounced topographic steering, which leads to collision at the outer bend and so forth. In conclusion, topographic steering enhances inner bend flow separation, while it obstructs outer bend flow separation (Blanckaert, 2018). These processes occurring in meandering rivers are schematized in Figure 1.

Topographic steering and the inflow conditions at the bend entry influence the angle at which the flow impinges with the outer bank. Hence, the adverse pressure gradient induced by the impingement and flow speed can either be enhanced or reduced by the inflow conditions of the flow (Ferguson et al., 2003). In a field study, Parsons (2003) found that the impingement angle correlates strongly with flow separation at both the inner and outer bend. Not only the onset of flow separation but also the size of the separation zone scaled with an increasing impingement angle (Parsons, 2003). Moreover, in a study using a numerical model, Hodskinson and Ferguson (1998) found that a large separation zone at the outer bank was related to the high velocity field being adjacent to the inner bank, while for a high velocity field adjacent to the outer bank at the bend's entry, no separation zone was present around the outer bend's apex. Hence, both the inflow conditions and the topographic steering can influence the impingement angle, which influences the occurrence and size of the separation zones. Nanson (2010) also found that the channel geometry and flow patterns at the entry of the bend influence the flow structure throughout the bend

1.1 Problem statement

Flow separation zones influence the hydraulics, ecology and morphodynamics of rivers. Flow separation zones decrease the effective width of the rivers and their conveyance capacity (Kleinhans et al., 2010). Hence, the bed patterns and the erosion patterns are influenced by the existence of separation zones (Kleinhans et al., 2010). Knowledge about these consequences can be applied to increase the accuracy of river models and to improve the management of rivers. Knowledge about the controlling factors of flow separation helps understand the deposition patterns more and predict the bend migration of meandering bends (Hodskinson and Ferguson, 1998; Kleinhans et al., 2010). Additionally, it is an important phenomenon to consider in the process of the re-naturalisation of rivers (Blanckaert et al., 2013; Kleinhans et al., 2010), since the process of letting straight rivers re-meander would lead to more separation zones. Because of this, the occurrence of flow separation is important in predicting the outcomes of environmental and civil engineering projects (Kleinhans et al., 2010).

Most studies regarding the controlling factors of flow separation are executed in a laboratory environment (e.g. Blanckaert, 2010; Blanckaert, 2015; Kleinhans et al., 2010) or use numerical modeling (e.g. Ferguson et al., 2003; Bo and Ralston, 2020; Kim et al., 2020), which use assumptions that are not applicable for natural rivers, such as a flatbed, symmetric bends or a constant width and radius throughout the bend. The studies that have used fieldwork to study flow separation are often focused on specific types of rivers, such as upland swamp channels (Nanson, 2010) or tidal meanders (Finotello et al., 2020). Other field studies research a limited amount of bends, such as Kasvi et al. (2013), which studied two bends, and Vermeulen et al. (2015), which studied a river bend with a deep scour hole. Therefore, the exact conditions for the onset of flow separation in natural, meandering streams, and the extent to which they influence the size of the separation zones remain unclear. The processes behind flow structures are not fully understood for simple bends, let alone for bends with more complex geometry (Engel and Rhoads, 2012).

1.2 Research aim and questions

The aim of the research is to evaluate the influence of potential controlling factors on the onset and size of flow separation zones. This will be done by evaluating the surface flow patterns throughout multiple bends in the Glanerbeek and comparing these patterns with findings from the literature. The Glanerbeek was selected because of its meandering structure, which allows for a good observation of the flow structure in the bends. The general surface flow pattern will be discussed, as well as the correlation between the separation zones and specific parameters. The following parameters are chosen because of their correlation with previous studies:

- Flow depth
- Radius
- R/B ratio
- Impingement angle
- Increase in cross-sectional area

A case study in the Glanerbeek will be executed to answer the main research question:

Which geometric and flow characteristics are controlling factors for the onset and size of flow separation in naturally meandering streams?

The following sub-questions will contribute to answering this question:

- How does the surface flow pattern in the bends differ with varying water levels?
- Which geometric characteristics of the river bends correlate with the size of the flow separation zones?
- What are the differences between inner and outer bend separation zones and their geometric and flow characteristics?
- How do these results correspond to controlling factors of flow separation observed in other rivers and laboratory studies?

1.3 Report outline

This report will start with a description of the methodology used to reach the research objective. This methodology consists of a description of the research area and the general methodology. Next, the results are presented. First, an analysis of the optimal settings for the research methods is studied in Chapter 3. Next, Chapter 4 discusses the general flow pattern of each bend, with an overview of the cross-sectional patterns per bend and includes a correlation analysis between the flow separation zones and the parameters described in Section 1.2. After the Results Section, the Discussion Section will reflect on how the findings from the study align with the literature. Moreover, the accuracy of the measurements is discussed and compared to measurements from the literature. Additionally, the Discussion Section will include the limitations of the research and recommendations for future research. Last, the Conclusion Section contains the concluding results of the research.

2 Methodology

This chapter will start with a description of the research area. Next, the general methods will be explained. The main method used in this research is the Large Scale Particle Image Velocimetry (LSPIV) method. For this method, it is required to have a seeded river and camera footage of this river. This will be elucidated in this chapter. Moreover, cross-sectional profiles are measured throughout the river section, which will also be explained in this chapter.

2.1 Research area

The research is executed in the Glanerbeek, which is a stream located in the border area between the Netherlands and Germany, near Enschede. This stream was selected because of its meandering structure, which allows for a good observation of the flow structure in the bends, which is of interest to this research. The total catchment area is 2281 hectares and the Glanerbeek has a length of 5.6 kilometres (Waterschap Vechtstromen, 2019). Flow velocities up to 0.5 m/s or higher are to be expected in the Glanerbeek (Provincie Overijssel, 2021). The width of the Glanerbeek is approximately five meters. The Glanerbeek starts within the Natura 2000 area Aamsveen in Germany and confluences with the Dinkel at Glane, in the Netherlands. The confluence with the Dinkel is located close to the research area. The section of the Glanerbeek that is used in this research, is a Natura 2000 area. Upstream of the research area, the water board is currently working on a re-naturalisation project (Waterschap Vechtstromen, n.d.). Figure 3 shows two photographs taken at the research area. A map of the research area is displayed in Figure 4.

Figure 3: Photographs of the Glanerbeek taken in the research. The flow direction is from the bottom to the top of the figure (taken by Mulder, I on 2-2-2024 (left) and 1-3-2024 (right))

2.2 Research methods

For this research, ten bends in the Glanerbeek have been selected. These bends were selected because they were located in a part of the river where there was not much canopy. Therefore, this river section was better visible with the drone and better accessible compared to other sections of the Glanerbeek. The river bends had various characteristics, which will be described in more detail in Chapter 4. The measurements were executed on three different days. During each of these days, camera footage has been taken from each bend. In addition to the camera footage, cross-sectional profiles were measured with real-time kinematic positioning (RTK), which can measure the position with an accuracy of centimetres making it one of the most precise technologies for obtaining positioning data (Takasu and Yasuda, 2009). The analysis includes

Figure 4: Map of the research area, with the names of the bends included. The flow direction is in the upward direction

cross-sectional profiles, which were measured just once per location, and camera footage of each bend, which were taken on each of the measurement days, each with different water levels. The dates of the measurement days were:

Table 2: Overview of the measurement days and the accompanying dates

	Measurement day 1	Measurement day 2	Measurement day 3
Date	01-03-2024	08-03-2024	18-03-2024

2.2.1 Cross-sections

For each river bend, three cross-sectional profiles were taken. These profiles were taken at the beginning of the bend, at the crest of the bend and at the end of the bend. Since the river bends were adjacent, the end of one bend indicates the starting point of the next bend. In total, 23 cross-sectional profiles were measured. These cross-sections were taken over the three different measurement days. These profiles were taken with the use of RTK technology (Figure 7), which determines the location of the measurement points. The approximate amount of measurement points required for a proper analysis was based on research of Geertsema et al. (2020), who also measured cross-sectional profiles in a Dutch stream. Translating the number of measurement points from Geertsema et al. (2020) to the Glanerbeek resulted in an average amount of 16 measurement points for the Glanerbeek. In the end, the average number of measurement points per cross-section was 14. The measurements were taken over a time span of three weeks (Table 2). According to expert's advice (personal communication), this timescale will likely not have a significant influence on the bathymetry of the bed of the stream.

2.2.2 Seeding

After the selection of the bends, a net was spanned across the width of the river (Figure 5). This net was initially spanned to catch artificial tracers. However, it was found that by shaking the net slightly, bubbles were created that followed the flow of the stream. These bubbles were chosen to be used as tracers in the LSPIV analysis. In this way, seeding with artificial tracers was not necessary, which reduces the probability of leaving artificial tracers in the water in case they bypass the interceptor. The net was placed at three to four different locations, to ensure sufficient tracers to occur in the river bends. This means that the tracers in a certain river bend could have been created just upstream of the bend, or at a location a few bends upstream of the bend in consideration. The tracers usually remained present over the length of four to five bends, although the number of tracers was gradually decreasing over the length of the river. Therefore, the net was replaced more often than strictly necessary, to ensure sufficient seeding at each bend. Light movement of the net was required to create tracers at the water surface. On the first measurement day, the tracers were generated by moving the net up and down on one side of the river. On the second measurement day, this movement was created while standing in the middle of the river, causing an obstruction to the flow. On the third and last measurement day, the movement was generated by two people moving the net on each side of the river, which can be seen in Figure 6. Additionally, the movement was generated by standing in the middle of the river, to test the difference in measurement outcomes. In the end, the measurements taken while standing in the river were not used in the analysis. A summary of the tracer-generating method used per day is given in Table 3.

Table 3: Tracer-generating method per measurement day

Day:	Day 1	Day 2	Day 3
Method	Net fixed on one bank, net shaken on the other bank	Standing inside the river	Standing inside the river, and: Net shaken on both banks of the river

Figure 5: Photograph of the net that was spanned across the Glanerbeek to create natural surface tracers (taken by Mulder, I. on 2-2-2024)

2.2.3 Drone Footage

The videos were taken per river bend. These recordings were made with a DJI Phantom 4 drone. The videos were made in 4K, with 3840 x 2160 pixels and the Field of View (FOV) is 84°. The flying height of the drone was 30 meters. The length of each video was around 1 minute. Ground Control Points (GCPs), were placed at the banks of the river bends (Figure 7). It was ensured that at least two GCPs were visible in each drone footage. These GCPs can be used for georeferencing, calibration and as anchors in the stabilization process.

2.2.4 LSPIV analysis

LSPIV depends on tracing particles at the surface of the flow, with which the surface flow velocities can be derived. This is done by applying cross-correlation between parts of the image patterns, called interrogation areas. From these cross-correlations, vectors are computed. This method is based on the assumption that the tracers do not change their position relative to other tracers within the time interval of the cross-correlation (Tauro et al., 2017). The accuracy of the method is mostly dependent on the visibility of the tracers in the river, their density (Dal Sasso et al., 2018) and reducing the aggregation of the tracers (Pizarro et al., 2020b). An increase in the seeding density reduces the error up to a certain point, after which the error increases again with a further increase of the seeding density (Meselhe et al., 2004). The increase at a higher density is likely caused by an accumulation of tracer particles which reduces the accuracy of the measurements (Pumo et al., 2021). The method is generally more accurate in rivers where tracers occur naturally (Tauro et al., 2018). Furthermore, the tracers should be spread out over the river surface for accurate measurements (Tauro et al., 2017).

After the video footage was extracted from the drone, this was used as input for the LSPIV analysis. This analysis was executed with the open software PIVlab (Thielicke and Stamhuis, 2014). Before the analysis, the most suitable frames were selected with the use of the Seeding Density Index (Pizarro et al., 2020a). This approach will be further elaborated in Section 2.2.5. After that, the videos were shortened to contain only these frames, for the stabilization of the video. The stabilization process was executed with a MATLAB script, using the Computer Vision Toolbox (MathWorks, 2021a) and Image Processing Toolbox (MathWorks, 2021b), where the GCPs acted as anchors. In other words, the GCPs acted as stable points that could be detected by the video reader within MATLAB.

Figure 6: Aerial view of two people moving the net on both sides of the stream. On the right side of the figure, the location of the GCPs is presented (taken from the drone footage on 18-3-2024)

Figure 7: On the left, a photograph of the measurements with the RTK at the Glanerbeek. On the right, an example of the placement of the GCPs (taken by Mulder, I. on 1-3-2024 (left) and 23-1-2024 (right))

The stabilized shortened videos were the input files for PIVlab. Next, the amount of frames used for the analysis has to be set. In this case, the number of frames per second, in other words, the sampling frequency, was set to 5 Hz. The selection of this parameter is described in Section 3.1. Next, PIVlab requires the definition of a mask or region of interest (ROI). The masks exclude areas from the analysis, while the ROI selects the region that should be analysed. The ROI can only be set to a rectangular shape, which is not applicable for the river bends. Therefore, it was chosen to use only the masks, which indicates all the areas that should be excluded from the analysis, which is mainly the banks of the river. The vegetated areas of the river were also excluded from the river because they would result in an inaccurate calculation of the surface flow velocity (Creëlle et al., 2018). Although the videos were stabilized, there was still some movement within the videos. Because of this, the masks sometimes needed to contain some of the river to ensure proper coverage of the vegetation during the entire duration of the video.

After the selection of the masks, the interrogation area had to be set. The selection of this parameter is elucidated in Section 3.1. Next, the distances in the video were calibrated with the use of the GCPs (Figure 7). This calibration was done by measuring the distances between the GCPs during the measurements. This real distance can be added to the results in PIVlab. The time between the frames was calculated with the use of the sampling frequency. With this calibration, the vectors calculated by PIVlab were transformed from px/frame to m/s.

2.2.5 Seeding Distribution Index

The Seeding Distribution Index (SDI) is a metric proposed by Pizarro et al. (2020a) to reduce the errors in the application of LSPIV in streamflow monitoring, especially those with relatively low seeding. The idea is to select the most informative frames instead of the entire video. In this way, noise and computational time are simultaneously reduced. The temporal window selected is based on the SDI, which combines the following seeding characteristics: seeding density, spatial clustering, spatial variance and the number of tracers. This method was proven to be successful in multiple studies (Pizarro et al., 2020a, Pizarro et al., 2020b and Dal Sasso et al., 2020). The SDI is calculated as:

$$SDI = \frac{D_*^{0.1}\rho_{cv1}}{\rho} \tag{7}$$

Where D_* is the dispersion index, ρ_{cv} is the reference seeding density, calculated to be $1.52 \cdot 10^{-3}$ particles per pixel (ppp) (Pizarro et al., 2020b) and ρ_s the seeding density in ppp. First, the videos were exported to image frames, which were the input of the MATLAB script provided by Pizarro et al. (2020a), to calculate the dispersion index, seeding density and with that the SDI . The original videos taken from the drone footage have a length of approximately one minute, with 60 frames per second. The SDI is calculated per frame and with this information, the frames with the lowest SDI values can be used to select the range of video frames that contain the most valuable seeding. These frames will then be used as input for the LSPIV analysis.

2.3 Optimization of research methods

The optimization will be based on the Mean Bias Error (MBE), Root Mean Square Error (RMSE), Normalized Mean Bias Error (NMBE) and the Normalized Root Mean Square Error (NRMSE). The MBE is calculated to find whether the LSPIV calculations over- or underestimate the velocities, based on the reference velocities measured by the float method. With the float method, a single tracer is tracked over a certain distance. This is done by manually timing how long a tracer is travelling over the distance. In this case, it is one of the tracers generated by the net. Next, the distance travelled is divided by the time spent over this distance, resulting in the velocity (Liu et al., 2021). This is done for ten different tracers per location. In this study, the tracers were tracked manually with the drone footage. This method has been used because the application does not require additional resources and was also used in a similar study by Sharif (2022). The MBE calculated with the reference velocities can result in either a positive or negative value. A positive MBE indicates that the LPSIV underestimates the velocities and vice versa (Legleiter and Kinzel, 2020). The MBE is calculated as:

$$MBE = \frac{1}{n}\sum_{i=1}^{n}(U_c - U_r) \tag{8}$$

Where n is the number of reference velocities, U_c is the calculated value by the LSPIV analysis and U_r the value of the reference velocities measured with the float method. The RMSE is calculated as:

$$RMSE = \sqrt{\frac{1}{n}\sum_{i=1}^{n}(U_c - U_r)^2} \tag{9}$$

The normalized versions of the MBE and the RMSE are calculated by dividing the not-normalized value by $\overline{O_i}$, which denotes the average value of the reference velocities. The NMBE and NRMSE are displayed in percentages [%].
The NRMSE and NMBE were calculated at different reference points, which were located before and after the bends. At each location, ten measurements were taken to calculate the average reference velocity. These reference velocities determined by the float method were compared with the LSPIV calculations to calculate the NRMSE and NMBE. An overview of the locations of the reference points is displayed in Figure 8.

2.4 Estimation of river bend characteristics

In this section, the methodologies used to estimate the characteristics of the river bend are elucidated. These will be used to test whether there is a correlation between the characteristics and the size of the flow separation area. The area of flow separation is measured within PIVlab, by drawing a polygon over the areas of flow separation. Often, it is not clear what the exact location and size of the flow separation areas are. For example, because part of the presumed area of flow separation is excluded by the mask. Therefore, the area of flow separation contains a minimum and a maximum value. The minimum value denotes the area of the surface flow where it is certain that there is flow separation. The maximum value includes the potential areas of flow separation.

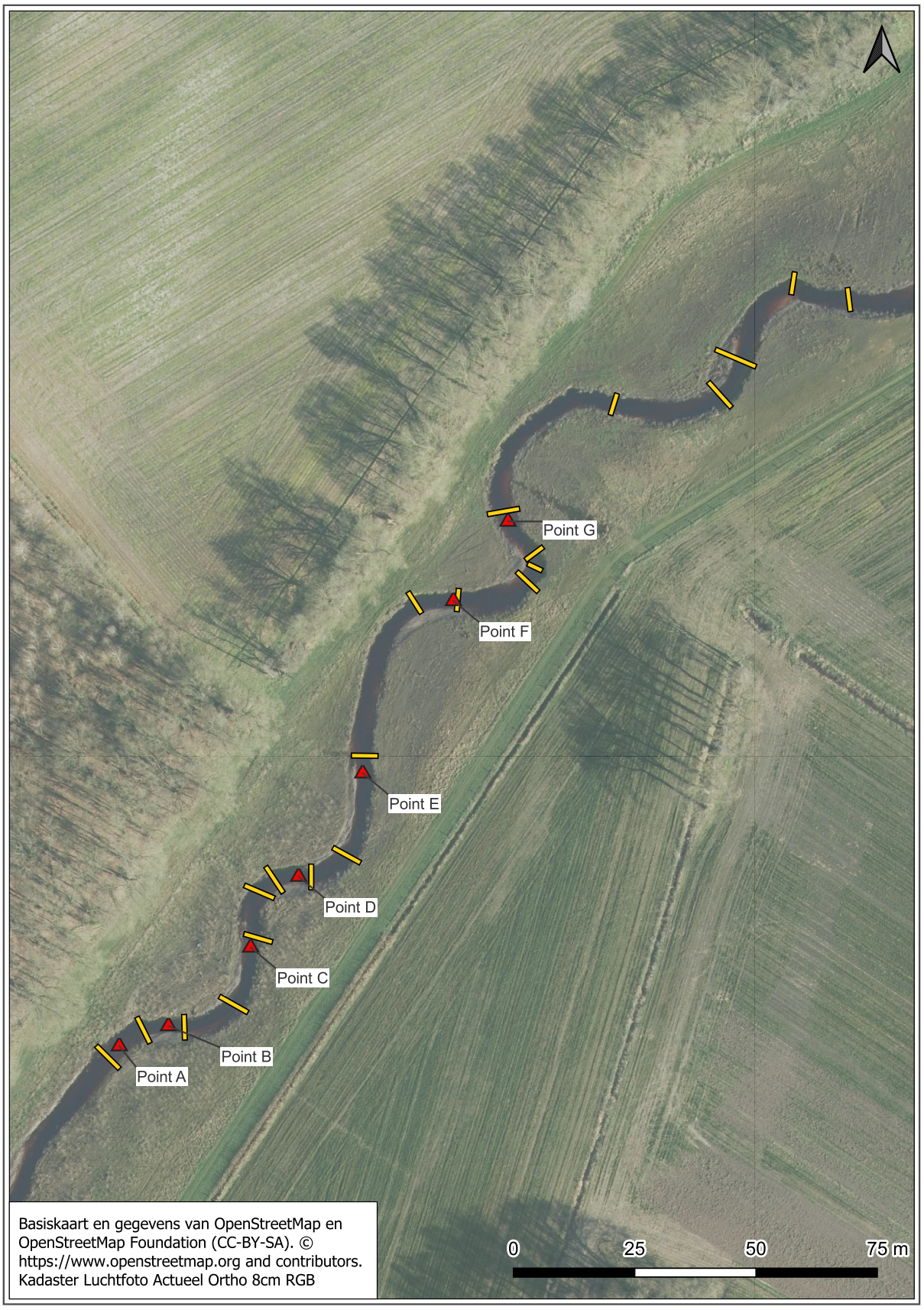

Figure 8: Map of the locations where the reference velocities for the sensitivity analysis are taken. The points taken with the RTK are displayed as the yellow stripes

2.4.1 Flow depth

To approximate the flow depth, RTK measurements were taken at the water level on both measurement days. The locations of these RTK measurements differed approximately 90 meters between measurement day 1 and measurement day 3. The flow depth that is measured is the datum of the water with regard to the Amsterdam Ordnance Datum (NAP).

2.4.2 Radius of the river bend

The radius of the river bend is calculated with the RivMap Toolbox (Jon, 2024). This is a script that calculates the curvature by determining the centerline and the width of the river bends from the aerial photos. The curvature is calculated at multiple points throughout the centerline. The average of the curvature values has been taken from the beginning to the end of the bend. The radius is calculated as $Radius = \frac{1}{Curvature}$

2.4.3 R/B ratio

The width of the river is also calculated with the RivMap Toolbox, from which the average value had to be calculated over the river bend. With this value, the R/B ratio was calculated.

2.4.4 Impingement angle

In Figure 9, the definition of the impingement angle is displayed. This impingement angle was measured with the use of the surface flow patterns of each bend. It should be noted that the impingement angle used in this study is an estimation of the impingement angle, to obtain a relative difference between the bends, rather than on the different measurement days.

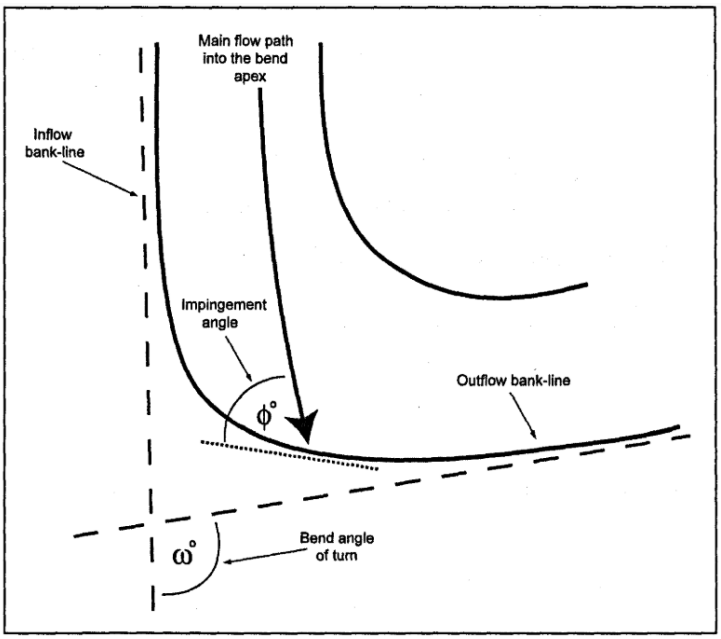

Figure 9: Schematic overview of the impingement angle, which is denoted as Φ. (Parsons, 2003)

2.4.5 Increase in cross-sectional area

The cross-sectional area was calculated with the cross-sectional profiles taken with the RTK. To determine the amount of increase in cross-sectional area, the difference between the area of the cross-sectional profile at the entry of the bend and the area of the cross-sectional profile at the apex of the bend was calculated.

3 Results of research methods optimization

In this chapter, the optimization of the research methods will be discussed. First, the characteristics of the placement of the net will be discussed. Here, the focus will be on the effect on the accuracy of both the distance of the net and the effect of the method for generating the tracers at the surface of the water. The second part of this section contains the influence of the most important settings for the LSPIV analysis: the sampling frequency, the video length and the interrogation area. The parameters selected for the optimization analysis are based on the research of Sharif (2022), who demonstrated the most important parameters for this kind of research.

3.0.1 Error metrics

In this section, a sensitivity analysis of the different methods for generating the tracers will be presented, as well as the influence of the distance from the net. For each placement of the net, the NRMSE was calculated with regard to reference velocities taken with the float method. More information for each location is found in Table 4, 5 and 6. These tables include the number of bends from the net, as well as the distance from the net. As can be seen, the net was not placed at the same locations for the different measurement days. Also, the tables show that at some locations, multiple measurements could be taken because of a relocation of the net, allowing for two separate values of error metrics at this point. This allows for a comparison between the placement of the net nearby and far away from the measurement point. As can be seen, the LSPIV method tends to underestimate the velocities in the stream, as the NMBE is mostly positive.

Table 4: Values of the NMBE and NRMSE between the reference velocities with the float method and the velocities calculated with LSPIV, per location for measurement day 1. Each point denotes a reference location. When there are multiple values present for a point, the reference location was visible on two videos, both with a different distance from the net. The distance from the net is displayed in the number of bends and in meters (calculated through the centerline)

Point	**A**	**B**	**C**	**D**		**E**	**F**	**G**
Bends from net	0	1	2	3	0	1	2	3
Distance from net [meters]	7	11	33	53	2	20	58	79
NMBE [%]	-22	+62	+28	-14	-6	+63	-16	+70
NRMSE [%]	29	39	24	19	10	40	21	12

Table 5: Values of the NMBE and NRMSE between the reference velocities from the float method and the velocities calculated with LSPIV, per location for measurement day 2. Each point denotes a reference location. When there are multiple values present for a point, the reference location was visible on two videos, both with a different distance from the net. The distance from the net is displayed in the number of bends and in meters (calculated through the centerline)

Point	**A**	**B**	**C**	**D**		**E**	**F**		**G**
Bends from net	0	1	2	3	0	1	2	0	1
Distance from net [meters]	7	11	33	53	2	20	58	3	24
NMBE [%]	+35	+93	+336	+381	+37	+351	-4	-12	+380
NRMSE [%]	43	49	78	80	30	79	11	16	81

Table 6: Values of the NMBE and NRMSE between the reference velocities and the velocities calculated with LSPIV, per location for measurement day 3. Each point denotes a reference location. When there are multiple values present for a point, the reference location was visible on two videos, both with a different distance from the net. The distance from the net is displayed in the number of bends and in meters (calculated through the centerline)

Point	**A**	**B**	**C**	**D**		**E**		**F**	**G**
Bends from net	0	1	2	3	0	4	1	2	3
Distance from net [meters]	2	6	28	48	2	65	20	58	79
NMBE (on two banks) [%]	-6	+10	+283	+176	+10	+114	-10	+5	-3
NMBE (standing in the river) [%]	-2	+28	+238	+115	-2	-39	-37	+12	+17
NRMSE (on two banks) [%]	8	14	75	64	10	92	13	10	9
NRMSE (standing in the river) [%]	8	23	71	55	12	64	61	14	17

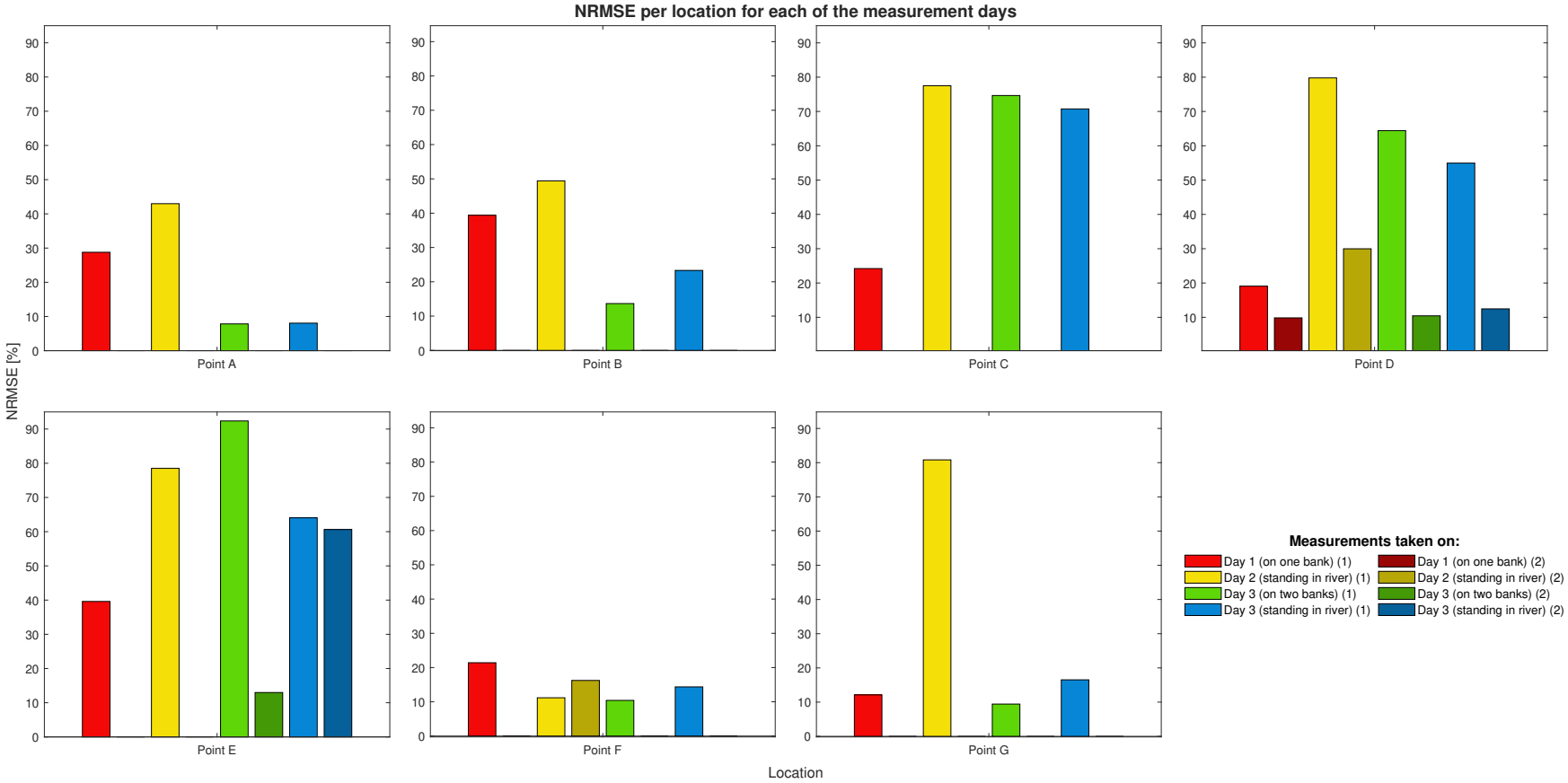

Figure 10: Net Root Mean Square Error (NRMSE) at the different reference locations for the three measurement days. The NRMSE is calculated between the reference velocities from the float method and the velocities calculated with LSPIV. Bars with a (1) denote the reference location is present in the first video, bars with a (2) denote when a reference location is visible in another video as well

3.0.2 Placement of the net

Figure 10 shows the NRMSE per location for each of the measurement days. The NMBE primarily gives an indication of whether LSPIV is under or overestimating the velocities. The NRMSE is more a metric to describe the accuracy of the calculated velocity, which is why only the NRMSE was plotted in Figure 10. As can be seen, at point D, E and F there are multiple results for one or more videos, which is why there are two bars present in Figure 10. This is because these points were filmed twice. The second time, the net was relocated closer to the points. Therefore, the bar graphs of points D, E and F show the influence of the placement of the net. At points D and E, the NRMSE is significantly lower for the videos where the net is placed closer to the reference point. The difference between the NRMSE for the two locations of the net is approximately between 10% and 80%. In point F, the NRMSE is lowest for the video where the net is located further away. However, it should be noted that this difference is considerably smaller, and the NRMSE is relatively low in both videos at point F during measurement day 2.

From this information, it would be expected that there is a positive correlation between the distance from the net and the NRMSE. In Figure 11 the distance from the net is plotted against the NRMSE. From this figure, it appears that there is no direct relationship between the distance from the net and the NRMSE. While the NRMSE is low for the shortest distances, similar values are found at other distances, for example right before the 60 and 80-meter distance, where there NRMSE for all measurement days is around 10 - 20%. More importantly, the pattern for day 2 and day 3 follows roughly the same pattern, as does day 1 at distances up to 20 meters. These results suggest that another factor is more important than the distance from the net.

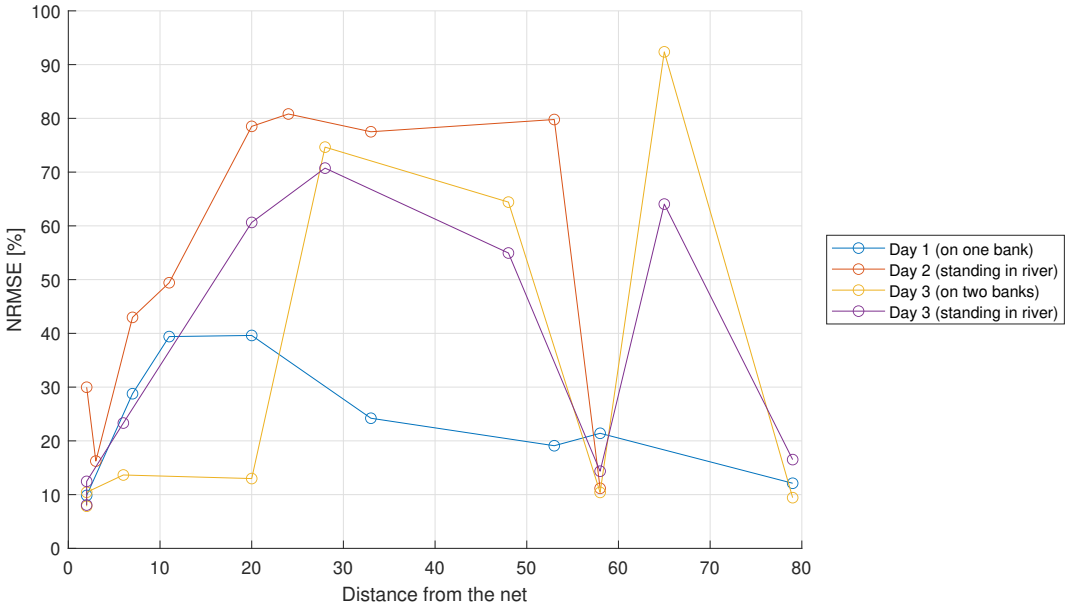

Figure 11: NRMSE at different distances, where each point denotes a reference point. The NRMSE is calculated between the reference velocities from the float method and the velocities calculated with LSPIV

3.0.3 Method for generating tracers

With the information from Table 3 and Figure 10, the sensitivity analysis can also be used to compare the different methods for generating the tracers. At five of the seven reference points, the NRMSE is highest for day 2, when the tracers were created while standing in the water. On day 3, the tracers were also generated while standing in the water, as well as standing on two banks. It would be expected that the NRMSE is higher while standing in the water. However, at points C, D and E, the NRMSE is higher for the measurements taken while standing outside of the water. The difference ranges from approximately 5% at point C to 30% at point E. At points B, F and G, the NRMSE is larger for the method while standing outside the water, ranging from 5% at point F to 15% at point B. At point A, the NRMSE has a similar value for both methods.

To better compare the errors for the different tracer-generating methods, the total NRMSE per day has been calculated. When there were multiple values of the NRMSE due to the existence of two reference velocities at one point, the average of these values was taken. The total NRMSE per measurement day is displayed in Figure 12. While it is apparent that the error is largest for day 2, the difference between standing on two banks and standing inside the water during day 3 is small. The NRMSE is lowest on day 1 when standing on one bank, but when applying almost the same technique during day 3, the NRMSE is a bit higher. More importantly, the difference in NRMSE is almost equal between 'Day 3 on two banks' and 'Day 3 in river', as it is between 'Day 3 in river' and 'Day 1 on one bank'.

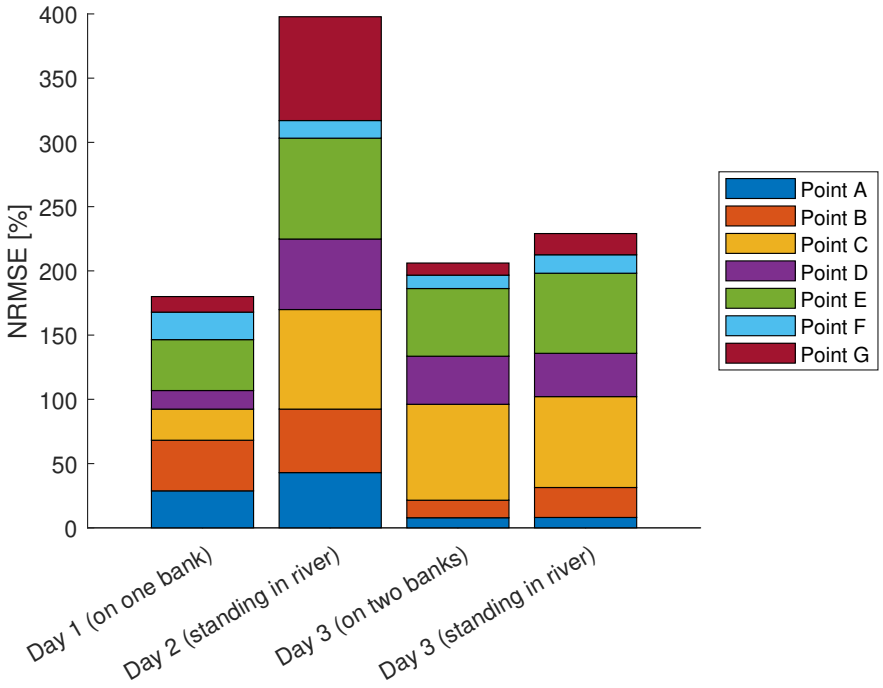

Figure 12: Total NRMSE of the reference velocities from the float method with regard to the velocities calculated with LSPIV, per measurement day

These findings make it difficult to draw a uniform conclusion regarding the influence of the tracer-generating method on the NRMSE. Adding to this, the reference velocities are also obtained through tracking particles at the surface. Therefore, it cannot be concluded that the difference in the NRMSE is necessarily caused by the tracer-generating method. It is likely that the differences in NRMSE are caused by other factors than solely the tracer-generating method. In the previous section, it was also concluded that the differences in NRMSE are not likely to be caused by the distance from the net. Therefore, it is important to be aware of other factors that could influence the differences in NRMSE. For example, the differences in properties at the reference locations, such as the local velocities, flow pattern and vorticity. Moreover, the float method is sensitive to human errors, because the reference velocities are measured manually with the footage of the drone. These human errors could be of a higher impact than the influence of the tracer-generating method and the distance from the net.

Although a consensus on the influence of the tracer-generating method could not be directly given after this sensitivity analysis, it is clear that the total NRMSE during day two is higher than on the other measurement days. Additionally. The obstruction of the person standing in the river likely influences the surface velocity pattern. Moreover, since the results of day 3 outside the river are better than the results of day 3 inside the river, the focus will be on the measurements without the person inside the river and the measurements of day 2 and day 3 inside the river will not be taken into account in this study.
One of the local properties of the reference points that can easily be analyzed is the influence of the velocities at the reference points on the NRMSE. In Figure 13, the NRMSE is plotted against the velocity. From this figure, it becomes apparent that there is a negative correlation between the NRMSE and the velocities up to a certain point. In other words, the NRMSE decreases with increasing velocity. The outliers that occur at velocities higher than 0.5 m/s, are mainly results from disregarded measurements.

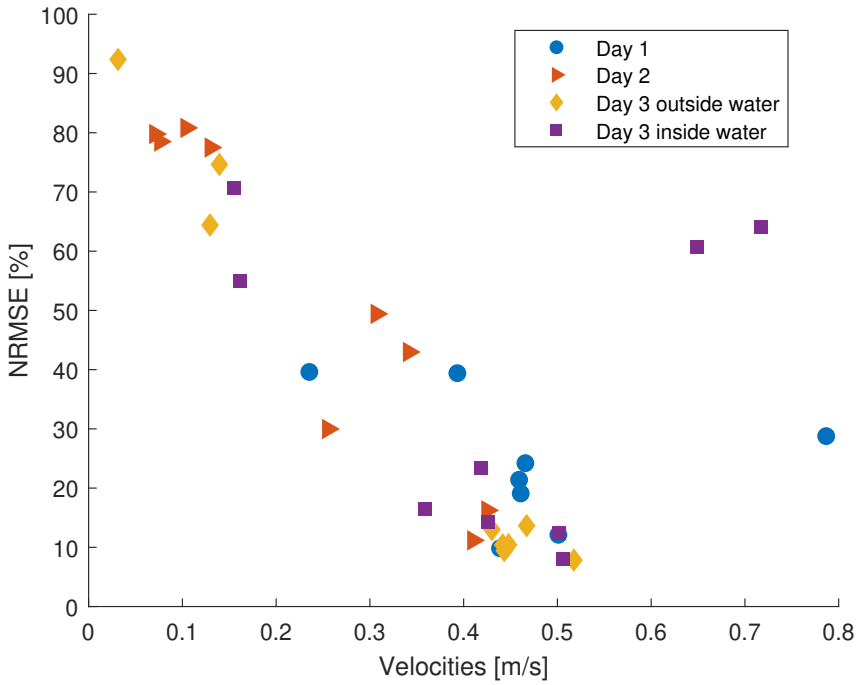

Figure 13: NRMSE plotted against increasing velocities. The NRMSE is calculated between the reference velocities and the velocities calculated with LSPIV. The velocities plotted are the velocities calculated with LSPIV at the reference points.

3.1 LSPIV settings

Approximately one month before the first measurement day, on 02-02-2024, a test measurement day was held. For this day, the natural tracers generated by the net were used as well. During this day, different methods of obtaining the data for the LSPIV analysis were tested. Moreover, the data collected during this day was used to find the optimal settings for the LSPIV analysis. This was done with the use of a sensitivity analysis which will be discussed below. The sensitivity analysis was performed on one video, which was obtained during this test day. The most important factors during this sensitivity analysis are the sampling frequency, video length and the interrogation area size. The parameters used during the sensitivity analysis of the three factors are summarized in Table 7.

Table 7: Parameters used during the sensitivity analysis. The tested values per parameter are denoted in the grey cells

Factor in sensitivity analysis:	Interrogation area	Video length	Sampling frequency
Interrogation area	16, 32, 64, 128, 256 pixels with a second and third pass	10 seconds	5 Hz
Video length	64 with a second pass	5, 10, 15, 30, 45, 60 seconds	10 Hz
Sampling frequency	64 with a second pass	15 seconds	3, 5, 7.5, 10, 15, 30, 60 Hz

One month before this test day, on 23-01-2024, another test day was executed at the river Dinkel, which is a river close to the Glanerbeek, but of a different size. There, the influence of the flying height and the stabilization of the videos were tested. This was done for three different videos: video A, B and C, which each had a different flying height, where video A had the lowest flying height and video C the highest. During this analysis, it was recognized that the most important feature of the flying height was to capture the entire river bend to get a full comprehension of the flow structure throughout the bend. It was chosen

that capturing the entire river bend was more important than the increased details that are provided with a lower flying height. Because the video is of 4K quality, there is the possibility of zooming in at a specific part of the video when desired, which remains in good enough quality to properly analyse the zoomed-in video with LSPIV. From this analysis, it was also found that the NRMSE between the reference velocities taken with the float method and the velocities calculated with LSPIV, decreased when increasing the flying height. Therefore, it was chosen to use a higher flying height and zooming in could have been a possibility when more details were required. It should be noted that, for this test day, the reference velocities at lower flying heights were taken at the reference points in recirculating areas, whereas the reference velocities at higher flying heights were taken over longer distances with more steady velocities at the reference locations. This could have been one of the reasons that the NRMSE was higher for lower flying heights. Therefore, these findings should be considered with caution.

The other part of the sensitivity analysis in the Dinkel regarded the effect of stabilization on the NRMSE. The reason for testing this effect was mainly because the stabilization process is time-consuming. From Figure 14, it can be found that for half the reference locations, the stabilization process improved the calculation of the velocities. The influence of the stabilization on the analysis is also a logical consequence, as the movement of the drone can either increase or decrease the perceived velocities of the particles. Together with the results in Figure 14 this led to the conclusion to stabilize each video in this analysis. Moreover, several papers indicate the stabilization process as an important parameter to increase the accuracy of LSPIV (e.g. Detert, 2021; Pearce et al., 2020; Pizarro et al., 2020b)

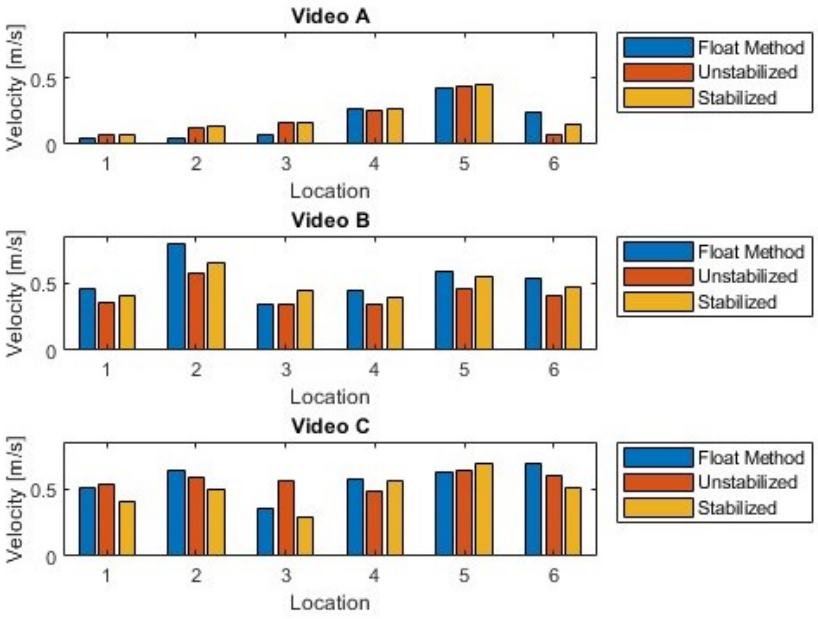

Figure 14: Comparison of the velocity approximated with the float method and the velocity calculated with LSPIV for three different videos taken at the Dinkel

3.1.1 Interrogation area

First, the optimal size of the interrogation area is tested. The interrogation areas are subdivisions of the figure, of which the cross-correlations are determined (Thielicke and Sonntag, 2021). As a rule of thumb, the number of particles within the interrogation area should be at least ten (Meselhe et al., 2004). PIVlab also has the option to select 'passes', which decreases the searching area of PIVlab for finding a cross-correlation between the tracer patterns. If the pattern is found in one of the smaller passes, PIVlab can stop searching for the pattern and thus requires less computational time (Thielicke and Stamhuis, 2014). The standard size of the pass is 50% of the higher pass. Thus the second pass is 50% of the interrogation area size, the third pass is 50% of the second pass and so forth.

In Figure 15, five different interrogation areas are tested. Each of these interrogation areas is also tested with a second and a third pass. It is clear that the RMSE is lowest for an interrogation area of 128 pixels. The RMSE decreases a bit when selecting the second pass. The influence of the interrogation area is relatively big, as it can decrease the RMSE up to approximately 0.3 m/s.

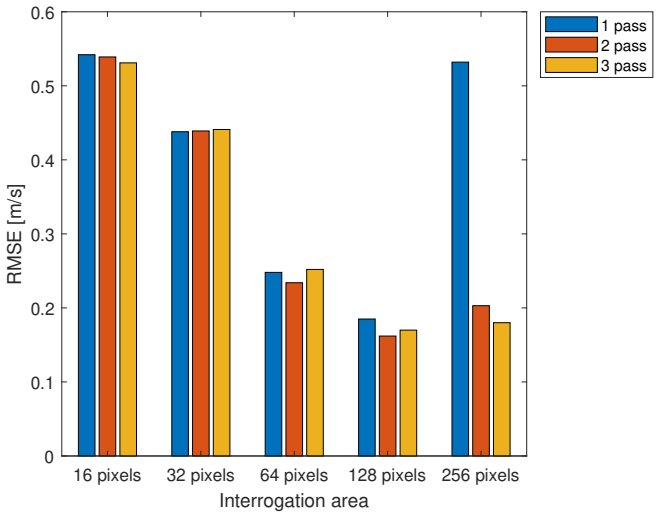

Figure 15: Influence of the interrogation area on the RSME. The RMSE is calculated between the reference velocities from the float method and the velocities calculated with LSPIV. Settings used: sampling frequency = 5 Hz and video length = 10 seconds

3.1.2 Video length

After the interrogation area, the optimal video length was tested. Increasing the video length is a way to decrease the error, especially in flows with low seeding density (Pumo et al., 2021). As a result of increasing the video length, the probability of having tracers in the entire ROI increases (Dal Sasso et al., 2020). However, in field studies, the probability of environmental disturbances also increases with increasing video lengths (Pumo et al., 2021). The original video lengths of each of the data was approximately 1 minute. The tested video lengths were 5, 10, 15, 30, 45 and 60 seconds. Compared to the sensitivity analysis of the interrogation area, the sampling frequency is changed to 10 Hz because less computational time was required to test the video length. The results are displayed in Figure 16. This figure shows that the RMSE is minimal for a video length of 10 seconds. However, it should be noted that the difference in RMSE is small, especially compared to Figure 15. Therefore, it can be concluded that the influence of the video length on the error is relatively small.

Looking at Figure 16, the optimal video length is 10 seconds. However, from experience, it is known that in areas where the particles are sparse, there are periods of time where there are almost no particles. Moreover, increasing the number of frames can benefit the composition of the surface velocity field over the entire section (Dal Sasso et al., 2020). Therefore, the chosen video length is 30 seconds. This increases the probability that there are particles within the sparsely covered areas.

As can be seen in Table 7, the time used to analyze the different interrogation areas was 10 seconds. This was mainly done to reduce the computational time of the sensitivity analysis. However, as mentioned before, the chosen video length is 30 seconds. While it was mentioned that the video length was not of much influence in Figure 16, the RMSE for the video length of 30 seconds was tested to be sure whether the error remains low for this length. It was found that the RMSE for a length of 30 seconds was 0.164 m/s, which is almost equal to the RMSE for a length of 10 seconds.

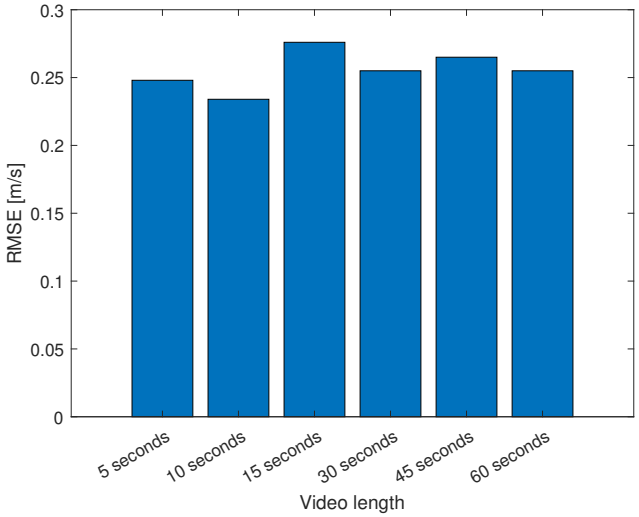

Figure 16: Influence of the video length on the RMSE. The RMSE is calculated between the reference velocities from the float method and the velocities calculated with LSPIV. Settings used: sampling frequency = 10 Hz and interrogation area = 64, with a second pass

3.1.3 Sampling frequency

Lastly, the optimal sampling frequency was tested. The sampling frequency can also be described as the number of frames per second and is given in Hz. Choosing the correct sampling frequency is important for the accuracy of the LSPIV analysis and is dependent on the flow characteristics of a river (Meselhe et al., 2004; Pumo et al., 2021). The original videos have 60 frames per second. For the sensitivity analysis, sampling frequencies of 3, 5, 7.5, 10, 15, 30 and 60 Hz were tested. Instead of the optimal video length of 30 seconds as found in Section 3.1.2, a video length of 15 seconds is chosen to reduce computational time. The results of the sensitivity analysis are found in Figure 17. From this figure, it is evident that the error is lowest for a sampling frequency of 5 Hz. The accuracy of LSPIV decreases with increasing sampling frequency, which was also found in the river Dinkel (Sharif, 2022). However, when the sampling frequency is too low, the displacements of the particles can outpace the searching area of the LSPIV and as a consequence, can lead to inaccurate velocities and thus increased errors (Meselhe et al., 2004). This likely causes the increase in error at 3 Hz compared to 5 Hz.

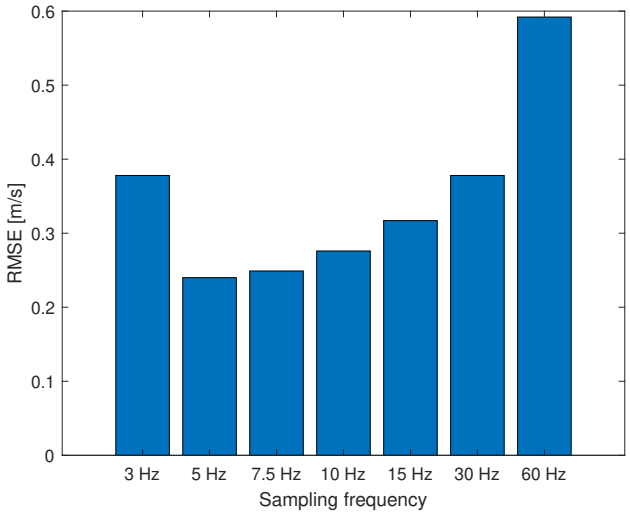

Figure 17: Influence of the sampling frequencies on the RMSE. The RMSE is calculated between the reference velocities from the float method and the velocities calculated with LSPIV. Settings used: video length = 15 seconds and interrogation area = 64, with a second pass

In the previous sections, the NRMSE has been discussed with the goal of finding the best settings for the LSPIV analysis and the best measurement days. In summary, the parameters that were used in the LSPIV analysis are displayed in Table 8. The analysis of the best settings for the LSPIV analysis was limited to changing one setting at a time and did not include the effect of a combination of multiple settings.

Table 8: Parameters used for the LSPIV analysis

Parameter	**Sampling frequency**	**Video length**	**Interrogation area**
Value	10 Hz	30 seconds	128 pixels, 2 passes

4 Results of field measurements

In this chapter, the results of the field measurements are presented. First, the general conditions on the measurement days will be described, including the water level and the weather characteristics. Next, the results per bend will be described, consisting of the surface flow velocity patterns on both measurement days and the cross-sectional profiles. After that, the correlation between the bend characteristics and the flow separation zones will be elucidated.

On the first measurement day, the water level was 33.39 +NAP and on the third measurement day, the water level was 33.10 +NAP. So there was a difference of approximately 30 centimetres, for a maximum water depth of 1.15 meters on day 1 and 0.86 meters on day 3. In Figure 18, the discharges in the Glanerbeek are displayed. The discharges were measured at a location 2 km (in a straight line) upstream of the research area. As can be seen, there was high discharge before the first measurement day. The discharges were decreasing over the research period, with a small peak between day 2 and day 3. Therefore, the difference in water level can reasonably be attributed to the difference in discharge.

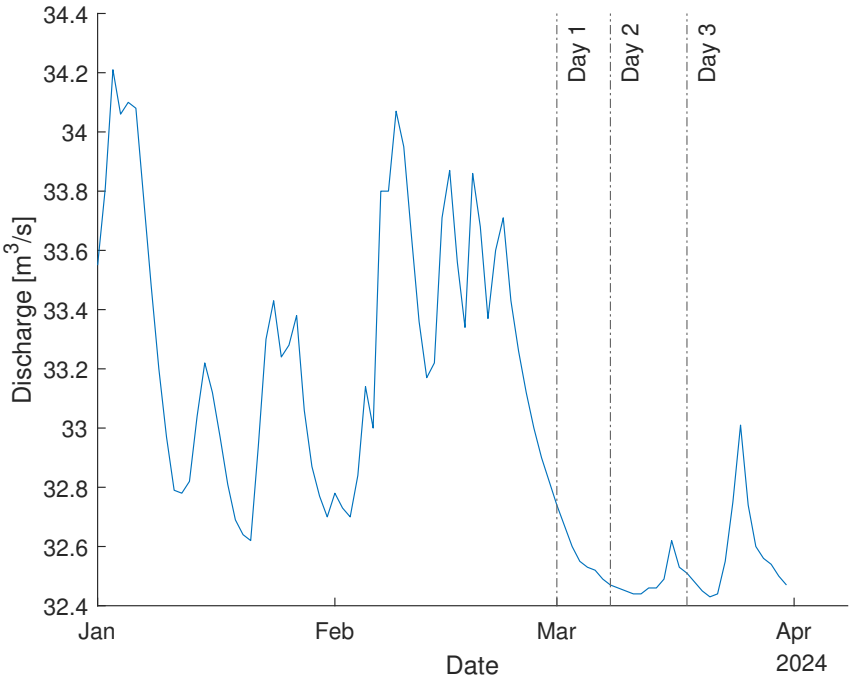

Figure 18: Discharges in the Glanerbeek in the first three months of 2024. The black lines denote the measurement days. (Source: Waterschap Vechtstromen, 2021-2024)

The weather characteristics during the measurement days are displayed in Table 9. The most significant difference between the measurement days is the cloud coverage. On days 1 and 3, there is complete overcast, while the sky is cloudless on the second measurement day. The global radiation is also significantly higher on this day. LSPIV is known to be sensitive to illumination conditions (Pumo et al., 2021; Tauro et al., 2017), such as shading (Pizarro et al., 2020b). This could have caused the increased error during the second measurement day, as described in Chapter 3. Additionally, the wind direction is eastward on the second measurement day, while the direction is more southward on measurement days 1 and 3. The average temperature and wind speed are highest on the first measurement day.

The seeding densities per bend are displayed in Figure 19. As can be seen, the densities range from 0 to 0.065 ppp and the densities are higher on the third measurement day.

Table 9: Weather characteristics on the measurement days. Data obtained from measurement station Twenthe (Koninklijk Nederlands Meteorologisch Instituut, 2024b). A wind direction of 360° degrees denotes a north wind (towards the south), 90° denotes an eastward wind, 180° a southward wind and 270° westward. The mean daily cloud cover is displayed as a number between 0 and 9, where 0 is a cloudless sky and with 9 the sky is invisible (Koninklijk Nederlands Meteorologisch Instituut, 2024a)

	Average temperature [°C]	Average wind speed [m/s]	Wind direction [°]	Mean daily cloud cover	Global radiation [J/cm^2]
Day 1	16	4.9	171	8	750
Day 2	14	4.1	90	0	1321
Day 3	14	2.2	200	8	575

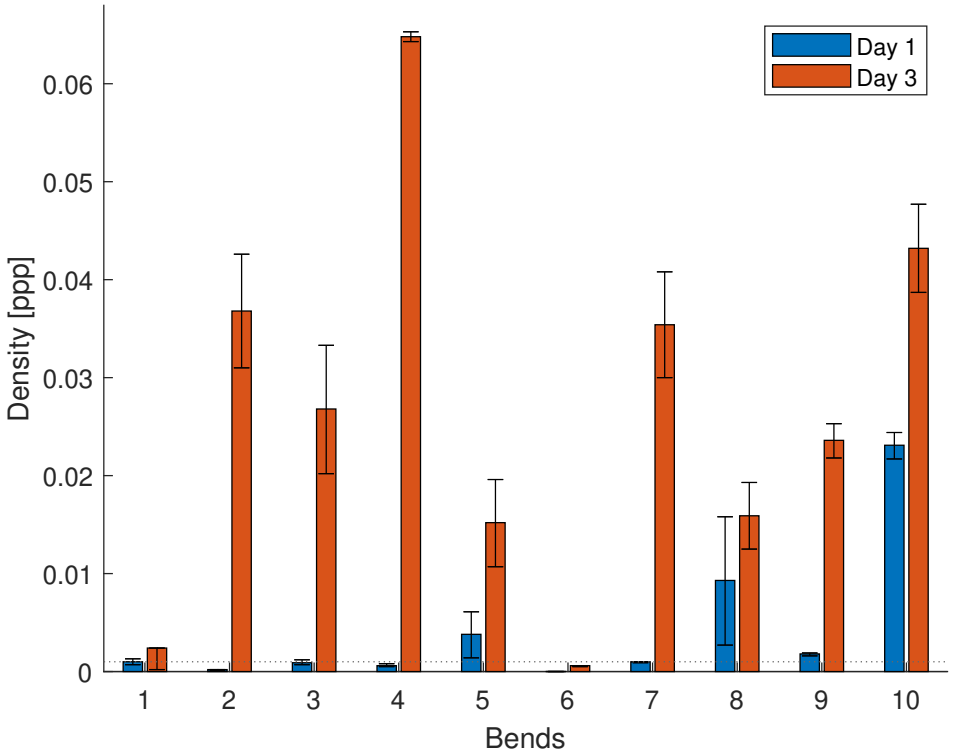

Figure 19: Seeding densities per bend for the two measurement days. The bar graphs denote the average densities during that day. The error bars denote the minimum and maximum seeding density that occurred during this day. The dotted line represents the minimum required seeding densities as determined by Pizarro et al. (2020a)

4.1 Results per bend

4.1.1 Bend 1

Figure 20 shows the surface velocities, cross-sectional profiles and the locations of the cross-sections for the first bend. The bend is considered to start downstream of cross-section A1 and end at cross-section A3, at which the next bend already starts. At cross-section A2, it can be seen that there is a small pool present around the apex of the bend.

When looking at the surface velocities, it is visible that the LSPIV analysis returns more information for the flow on the first measurement day. Although looking at the densities in Figure 19, it would be expected that there would be more information on the third measurement day due to higher densities. It is likely that there is an error in the results of day 3, as the surface flow pattern is looking odd. The maximum velocity during the first measurement day is approximately 0.06 m/s higher compared to the third measurement day. Higher velocities are to be expected on the first measurement day because of the higher water level and discharge during that day.

During the first measurement day, the high velocity field impinges on the outer bend right before the apex of the bend. Downstream of this point, a large area of flow separation occurs at the inner bank. The high velocity field remains close to the outer bank. During the third measurement day, the high velocity field does not seem to impinge on the outer bank. Instead, the flow is deflected in the direction of the bend. At the location of cross-section A3, an area of flow separation occurs. This separation zone will be further discussed in Section 4.1.2, as it is considered to be the entry of the second bend.

Another observation in the surface flow pattern is the outer area of flow separation right downstream of the net. This area is larger during the third measurement day. In Figure 20d, the location of the separation area on day 1 is located on the left-hand side of the figure, upstream of the location of the first cross-section. It can be seen that the bed at this location is higher than the bed in the middle of the stream and that the flow is shallow. Moreover, the flow contains partly submerged vegetation. This could be the cause of this small separation area at this location. It could explain why the separation area appears to be larger on the third measurement day, as the water depth was lower during this day and thus relatively more obstructed by the vegetation. Another explanation could be the shade from the vegetation on the outer bank. At this location, some small trees and bushes were present that caused some shade to fall on the stream. LSPIV is known to be sensitive to illumination conditions (Pizarro et al., 2020b; Pumo et al., 2021; Tauro et al., 2017). However, since the measurements were both taken in the morning and the illumination conditions in Table 9 are similar, this explanation is less likely as the location of the separation zones would be expected to be situated approximately at the same location.

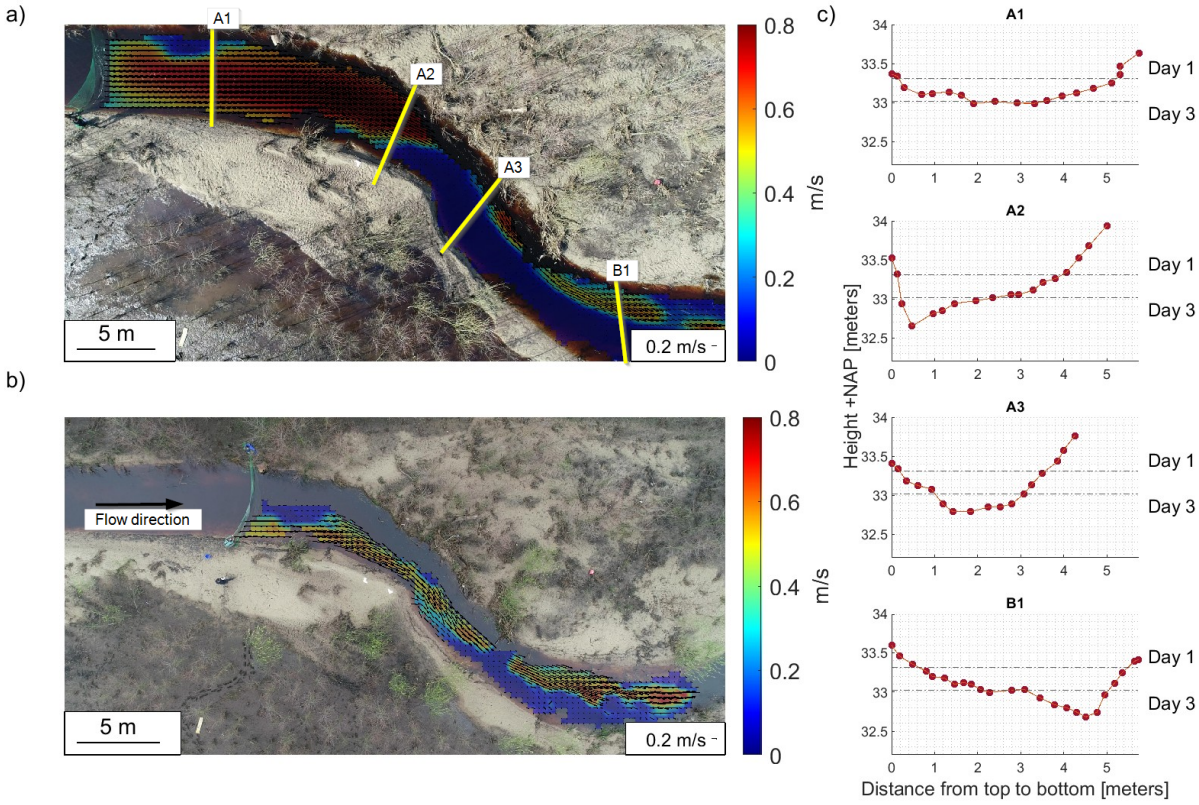

Figure 20: Surface flow velocities in bend 1 for day 1 (a) and day 3 (b), with the corresponding cross-sectional profiles displayed in (c), where the dots represent the RTK measurements. Bend characteristics are found in Appendix B and the size of the flow separation area in Appendix A

4.1.2 Bend 2

Bend 2 is displayed in Figure 21. The flow structures between the two measurement days differ, most notably around the apex of the bend. During the third measurement day, the main flow impinges on the outer bank, while the flow on the first measurement day is directed along the curvature of the bend. This difference is likely caused by topographic steering, which is more prevalent at lower velocities. Due to the direction along the curvature, there is no area of inner bend flow separation downstream of the bend's apex on the first measurement day. From cross-section B1 it can be observed that there is a large point bar present at the inner bank. On the first measurement day, there is flow over this point bar, while it goes around the point bar on the third measurement day. Since the cross-sectional profile shows that the flow over the point bar is not that shallow, this difference could be explained because the water level is higher on the first measurement day. Therefore, the flow is able to flow over the point bar during day 1. On day 3, the water level is lower, which forces the flow around the point bar. Due to this redirection, the flow separation zone is smaller at the outer bend and larger at the inner bend.

On day 1, there are some more gaps around the apex of the bend, which could have been caused by the large difference in seeding density between the first and third measurement days (Figure 19). Other than that, no distinct differences in the pattern of the LSPIV are noted that could be caused by this difference in seeding densities.

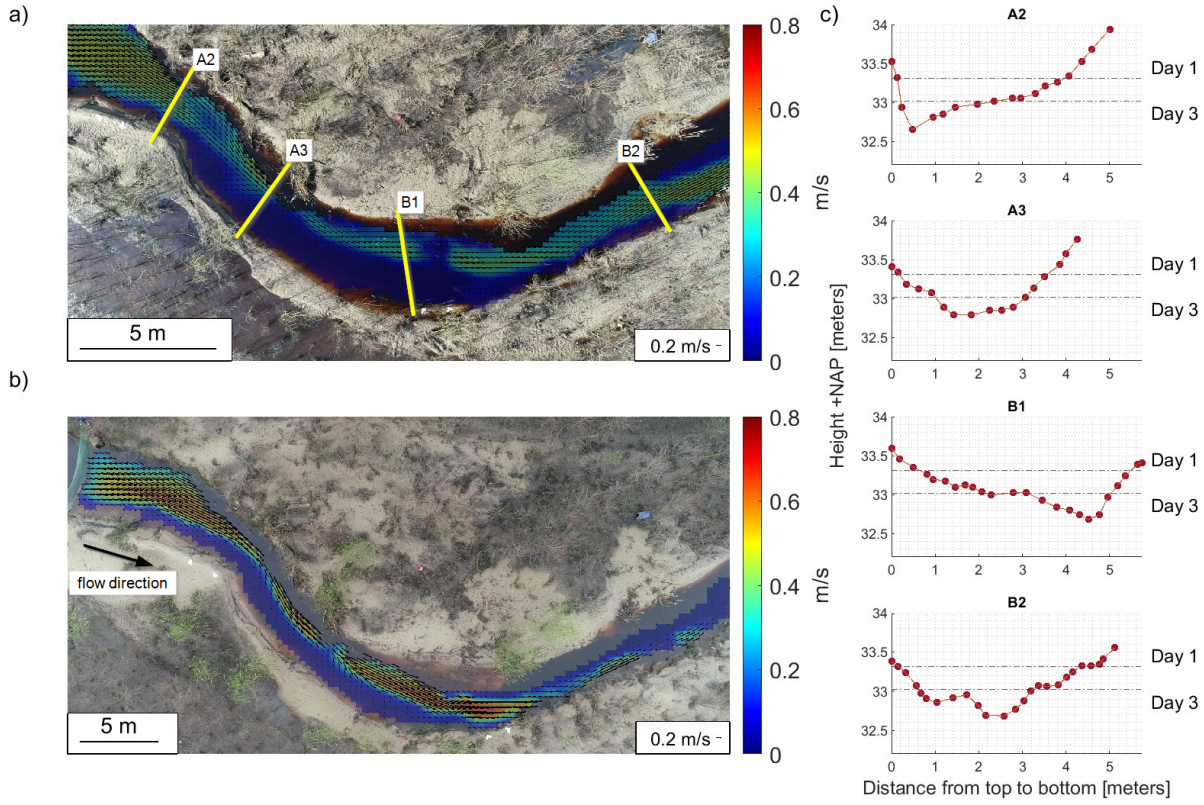

Figure 21: Surface flow velocities in bend 2 for day 1 (a) and day 3 (b), with the corresponding cross-sectional profiles displayed in (c), where the dots represent the RTK measurements. Bend characteristics are found in Appendix B and the size of the flow separation area in Appendix A

4.1.3 Bend 3

Figure 22 illustrates the surface velocities on day 1 and day 3, the location of the cross-sections and the cross-sectional profiles at these locations. The first thing that stands out is the difference in surface velocity patterns during day 1 and day 3. During day 1, the high velocity field is more spread out over the river, up until the point where the vegetation on the left bank obstructs the flow, and the high velocity field moves to the inner bend of the river. During day 3, the high velocity field, before the obstruction from the vegetation on the outer bank, is less visible. However, this could be caused by a mask on the right side of the stream. During this day, the high velocity field also seems to be obstructed at the same location. However, where the high velocity field seems to continue throughout day 1, during day 3 it seems to disappear, up until the crest of the river bend. When looking at the geometry of the stream, it can be seen that there is a slight increase in the width of the stream at this location. This could also result in reduced velocities. However, when there are areas of flow separation on both sides, it would be expected that due to the reduction in conveyance capacity, the velocity would remain high. Comparing cross-sections C1 and C2, it is likely that the increase in cross-sectional area also influences the reduced velocities.

The maximum velocity is approximately 0.2 m/s higher during day 1 compared to day 3. As the water level is higher during day 1, it would be expected that the velocity is somewhat higher. As the flow pattern on the third measurement day shows a lot of low velocity zones, there could be errors in the LSPIV analysis during this day. Looking at the densities in Figure 19, it would not be expected that these gaps are caused by the density. The occurrence of the gaps will be further discussed in Chapter 5.1.2.

The flow separation areas at this bend are located both on the inner and the outer part of the bend. On day 1, the outer bend separation area starts after the vegetation at the outer bank. At the same time, this is also the location where there is an expansion of the width of the stream. During day 3, the outer bend separation seems to start further upstream, after the exit of the former bend, bend 2. Because of a difference in drone footage between the different days, this part of the stream is not visible in this figure. However, in Figure 21 this area is visible. From this figure, it can be seen that during day 1, there was no flow separation after the exit of the bend. When looking more closely, it can be seen that the flow structure at the exit of this bend is different. During day 3, the high velocity field appears to swirl to the inner bank, right before the exit of the bend, while the high velocity field shows a uniform curve during day 1. This could be caused by the lower water level and velocity during day 3, so that the surface flow cannot flow over the bar at the inner bend of bend 2, causing the swirl in the high velocity field and obstruction of the flow at the exit of bend 2, which induces the flow separation zone at this location.

During day 1, there is a small inner bend separation zone at the crest of the bend. This seems to be induced by the vegetation right before the crest of the inner bend. After the crest, another area of flow separation starts. The high velocity field is moving forward in a straight line due to inertia. Therefore, the velocity in the expansion area is close to zero, as there is no 'need' for this water to flow in the direction of the expansion. During day 3, the separation area at the crest is less visible than during day 1. This could be caused by the lower water level, causing the point bar to be above the water level and therefore limiting the separation area. This point bar is visible in cross-section C2.

In the downstream part of the stream, the high velocity field is less present during the third day. It appears that the high velocity areas follow the outer bank more closely compared to the first day. This could be caused because of higher inertia on the first measurement day, directing the flow in a straight line through the bend.

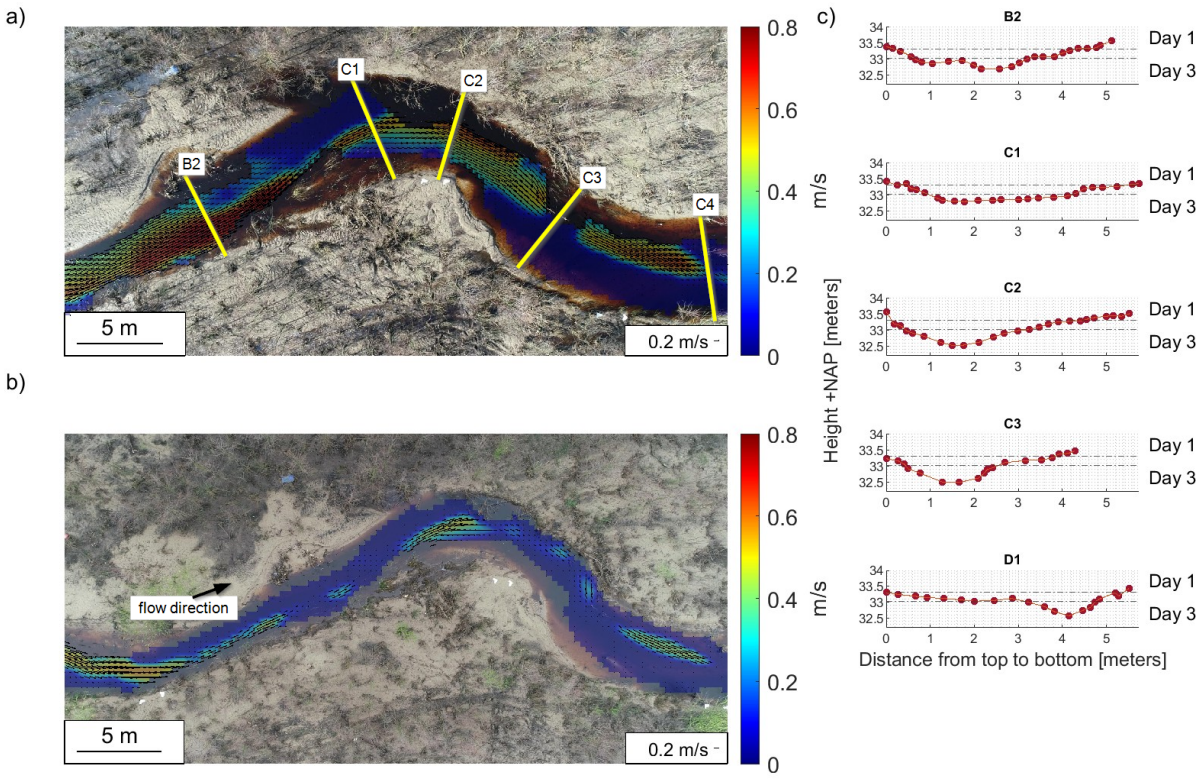

Figure 22: Surface flow velocities in bend 2 for day 1 (a) and day 3 (b), with the corresponding cross-sectional profiles displayed in (c), where the dots represent the RTK measurements. Bend characteristics are found in Appendix B and the size of the flow separation area in Appendix A

4.1.4 Bend 4

In Figure 23, the surface flow velocities are displayed for the fourth bend. The flow patterns are somewhat similar during the two measurement days. Both show outer bend separation downstream of the crest and inner bend separation upstream of the bend. Moreover, the maximum velocity is slightly lower (0.1 m/s) for the third measurement day, where the water level was lower. The cross-sectional profiles C2, C3 and D1 show that there is a pool and point bar present in the river bend. During both days, the velocity increases right up until the point of impingement with the outer bend. Comparing Figure 23 with Figure 22, it can be seen that the flow pattern on the third measurement day does not show as many gaps as in Figure 22. It is likely that there are some errors in the footage of the third bend.

The outer bend separation shows a similar pattern on both measurement days, likely being caused by inertia directing the high velocity field in a straight direction. The inner bend separation also seems to occur due to inertia, as it seems that the high velocity field is unable to follow the curvature of the bend. However, when looking more closely, it can be seen that the flow is obstructed by a vegetated point bar at the inner bend. This point bar is also visible on cross-section D1. Although the point bar is partly submerged during day 1, the vegetation is still capable of obstructing the flow.

Downstream of the crest of the bend, during day 3, gaps of low velocity are observed in the high velocity field. During day 1, there were some minor gaps observed in the high velocity field. The gaps could partly be caused by the placement of the mask at the vegetated outer bank. The possible explanations for the occurrence of the gaps will be further elaborated in Chapter 5.

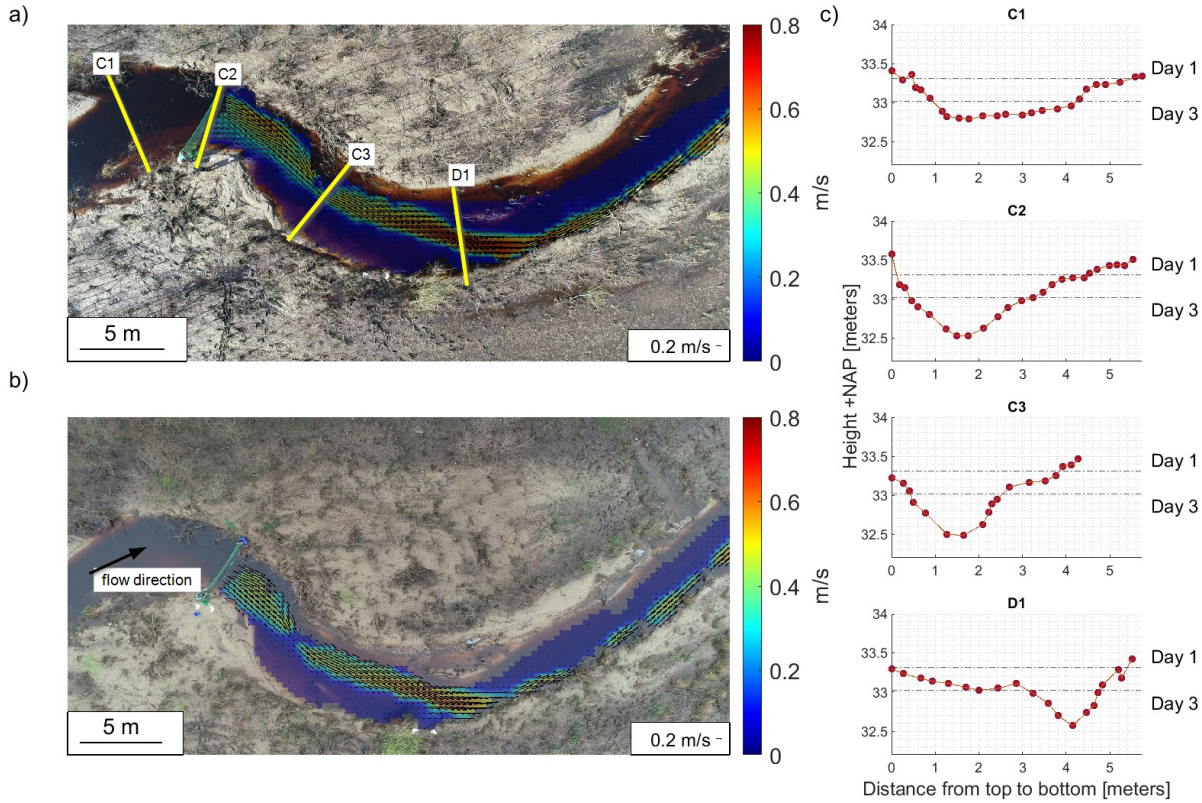

Figure 23: Surface flow velocities in bend 4 for day 1 (a) and day 3 (b), with the corresponding cross-sectional profiles displayed in (c), where the dots represent the RTK measurements. Bend characteristics are found in Appendix B and the size of the flow separation area in Appendix A

4.1.5 Bend 5

Figure 24 displays bend 5 and its accompanying surface flow velocities and cross-sections. As with most bends so far, the maximum velocity is lower for the third measurement day (0.05 m/s). The flow pattern during both days is similar. However, at the third measurement day, there is a gap upstream of the crest of the bend. At both bends, flow separation occurs at the inner bend. When following the flow from upstream to downstream, a small flow separation area is observed at the inner bank first for both measurement days. This could be caused by a small protrusion in the bank. Following the flow downstream, the high velocity field is redirected slightly to the inner bend, causing a small outer bend separation area during day 3. This change in direction is likely caused by vegetation at the outer bank. Right before the crest of the bend, the high velocity field becomes narrower which results in the onset of the inner bend separation area. This narrowing occurs during both measurement days. It could be caused by an increase in the bed level, as this is also the location where the sandy inner bank starts. In cross-section E2, a small increase in the bed level is found right before the bank starts. However, for a better understanding of the bed at the point of onset of flow separation, the bed at this location should be studied.

The high velocity field is located near the outer bank downstream of the crest of the bend. Subsequently, the flow separation area remains present until the end of these figures. In the next chapter, the reattachment point of the high velocity field to the inner bank of bend 5 (or outer bank of bend 6) will be elucidated.

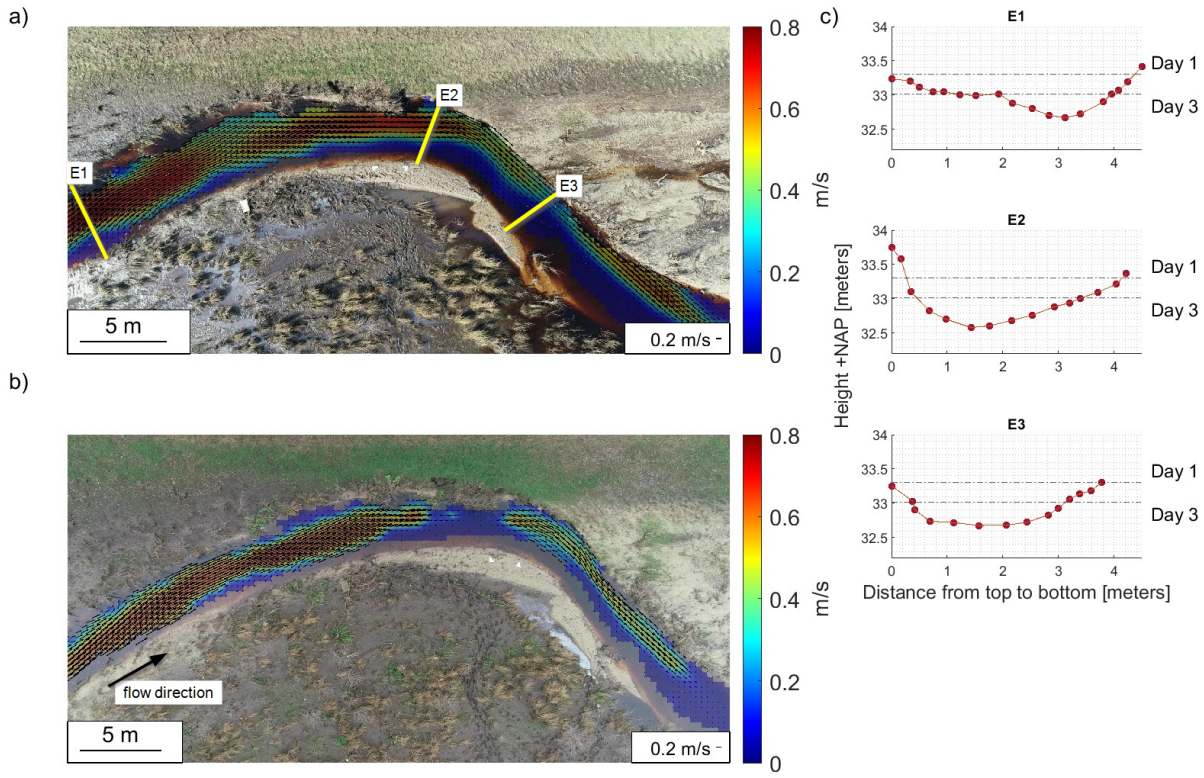

Figure 24: Surface flow velocities in bend 5 for day 1 (a) and day 3 (b), with the corresponding cross-sectional profiles displayed in (c), where the dots represent the RTK measurements. Bend characteristics are found in Appendix B and the size of the flow separation area in Appendix A

4.1.6 Bend 6

As mentioned in the previous section, the reattachment of the flow to the bank is visible in Figure 25. As can be seen in this figure, the high velocity field flows in a straight direction until it reaches the outer bank of bend 6 and reattaches to the boundary there. Also due to this motion, a detachment at the inner bank occurs. This marks the start of the inner bend flow separation area. Since the footage is taken from different viewpoints, the exact location of the inner bend separation area is difficult to observe. However, when looking at the vegetation, it seems that the onset starts slightly more upstream during day 1 compared to day 3. Moreover, when looking closely it can be seen that there is a slight deflection away from the inner bend at this point. This deflection is more distinct during day 1. Since this deflection occurs abruptly at this point, it is not likely that the deflection is only caused by the curvature of the bend. It is more plausible that the point bar that can be seen at the crest of the bend, is starting from this point and the deflection is caused by topographic steering. Since the water level was lower during day 3, the location where the flow separation was starting on day 1 was not inundated during day 3, causing the topographic steering to occur at a location closer to the crest of the bend. This causes a difference in the size of the flow separation zones.

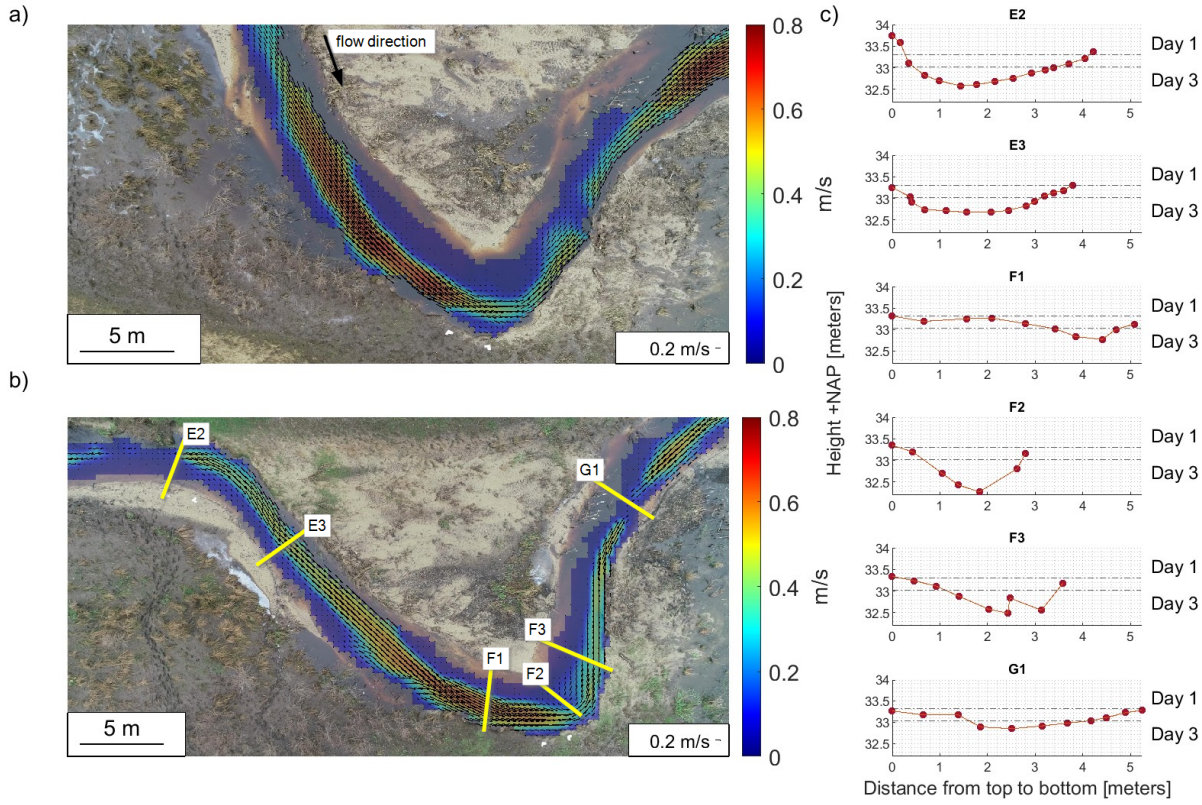

Figure 25: Surface flow velocities in bend 6 for day 1 (a) and day 3 (b), with the corresponding cross-sectional profiles displayed in (c), where the dots represent the RTK measurements. Bend characteristics are found in Appendix B and the size of the flow separation area in Appendix A

Furthermore, a re-circulation area is visible at the outer bend on the first measurement day. This is visible in more detail in Figure 26. On the third measurement day, there is a small area of outer bend separation, but recirculation cannot be observed. The high velocity field is flowing more towards the apex during day 3 compared to day 1, where the high velocity field seems to impinge on the outer bank downstream of the apex. However, these differences could also be exaggerated by a difference in the placement of the mask. The bank around the apex is steep (cross-sections F1 and F2), so the difference in the river bend that is submerged with the different water levels is small. In that way, the recirculation zone cannot have been caused by a larger submerged area during day 1, implying that the difference is caused by a different flow pattern.

The lack of reattachment of the high velocity field to the inner bank is likely caused by inertia, as it was in bend 5. During day 1, the area near the inner bank is not visible because it is excluded with the mask. It is expected that the flow separation continues throughout the area that is excluded by the mask, which contains submerged vegetation. During day 3, it can be seen that the flow separation area remains present

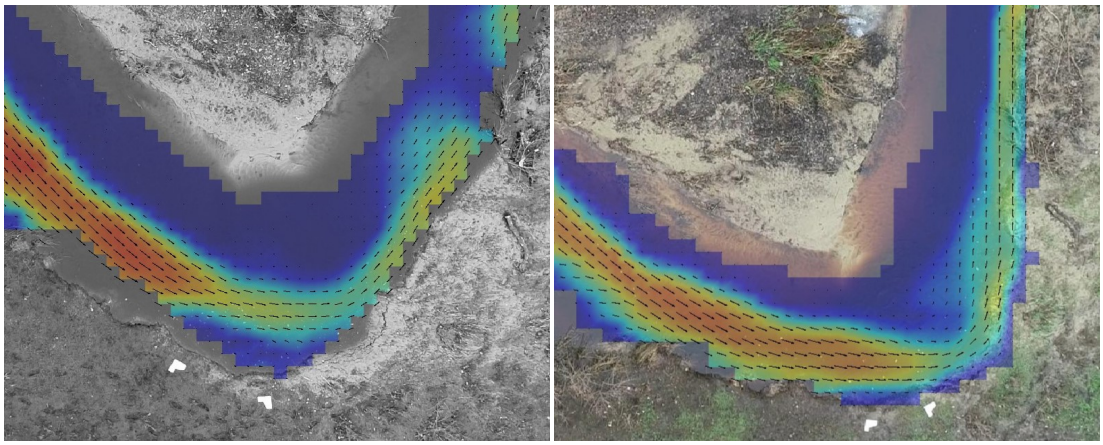

(a) (b)

Figure 26: Zoomed in figures of the surface flow in bend 6, on a) day 1 and b) day 3.

on the side of the inner bend through the end of the figure. The distance between the exit of the fifth bend and the entry of the subsequent bend is too short for the flow to expand over the width of the bend. Additionally, a small separation area seems to occur on the right side of the high velocity field, likely caused by inertia and the lack of widening over the channel width of the high velocity field.

Another observation that stands out at this bend is that the seeding density is low, especially during the first measurement day (Figure 19). This could have been caused by the sharpness of this bend, which attenuates all the tracers.

4.1.7 Bend 7

Bend 7, displayed in Figure 27, is an interesting case, as there are two distinctive flow patterns during the two measurement days. On day 1, there is a small separation area at the inner bend, around the crest of the bend. During day 3, the onset of flow separation occurs slightly more upstream and remains present throughout the length of the bend. For both measurements, the net is placed close to the bend. When comparing Figure 27a and b, there is not much difference in the inflow pattern, except for the high velocity field being wider on the first measurement day. Cross-section G1 shows a small point bar, which is inundated only on the first measurement day. It is likely that the difference in separation area is caused by the difference in water level and thus velocities throughout the river.

Another aspect that stands out in the surface flow pattern is the reattachment of the separation zone to the high velocity field. During day 1, this reattachment occurs close to the onset point of flow separation, while it does not occur within the range of the figure for the third measurement day. During day 1, the flow impinges with the outer bend more upstream compared to day 3. Due to this difference in impingement, the direction of the main flow differs slightly on both measurement days, which likely causes the difference in separation zones.

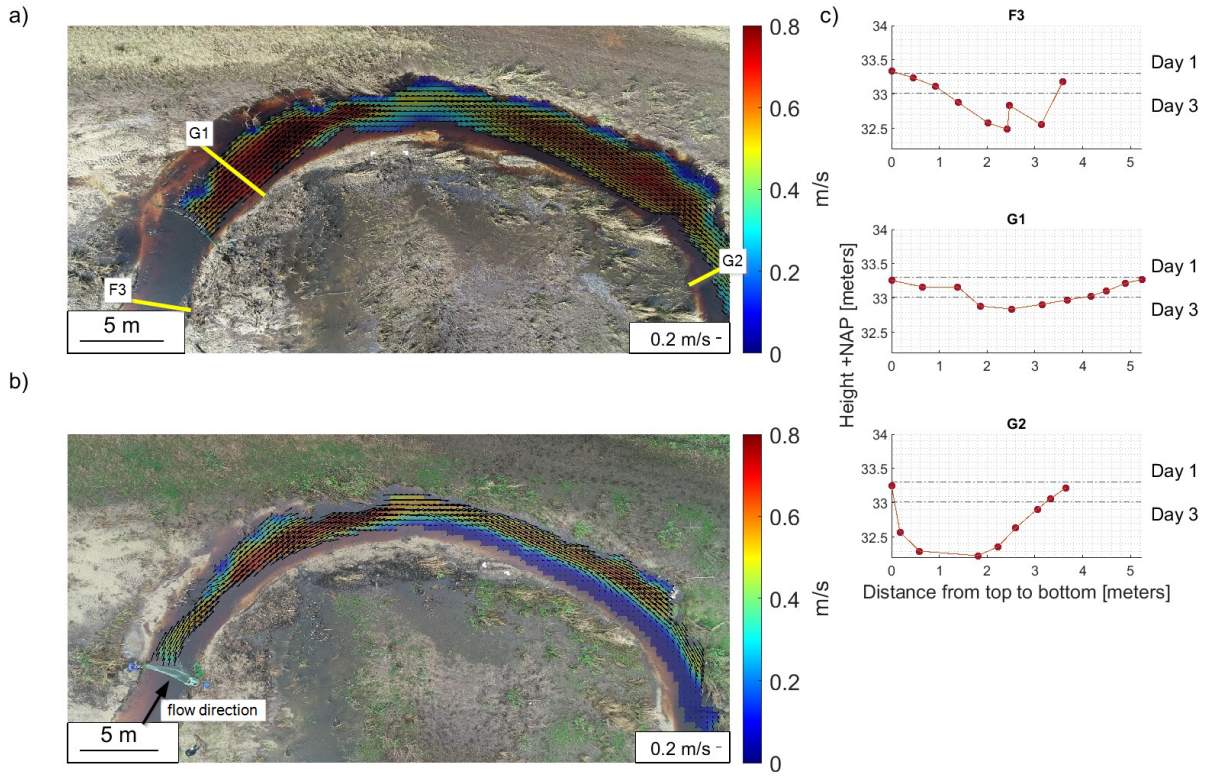

Figure 27: Surface flow velocities in bend 7 for day 1 (a) and day 3 (b), with the corresponding cross-sectional profiles displayed in (c), where the dots represent the RTK measurements. Bend characteristics are found in Appendix B and the size of the flow separation area in Appendix A

4.1.8 Bend 8

Figure 28 shows the surface patterns and cross-sections for the eighth bend. During day 1, there is no distinct outer bend separation area upstream of the bend's apex, because the reattachment point is close after the onset of the separation zone in bend 7. Hence, the inflow conditions differ between the measurement days. It can be seen that the main flow occupies the full width of the stream on day 1, where it is limited to a smaller width on day 3. The main flow on day 3 impinges with the outer bend upstream of the apex, after which it remains located along the outer bank until the protrusion of the outer bank downstream of the apex. Here, a small separation zone occurs on the outer bank since the main flow remains flowing in a straight direction due to inertia. Downstream of this point, the flow starts to expand again.

During day 3, the main flow impinges at a different location due to the inflow conditions. The impingement occurs at the apex of the bend. Since the flow was covering the entire width of the stream, the impingement caused the onset of a minor inner bend separation zone. An outer bend separation zone is developed downstream of the protrusion, at the same point as on the first measurement day.

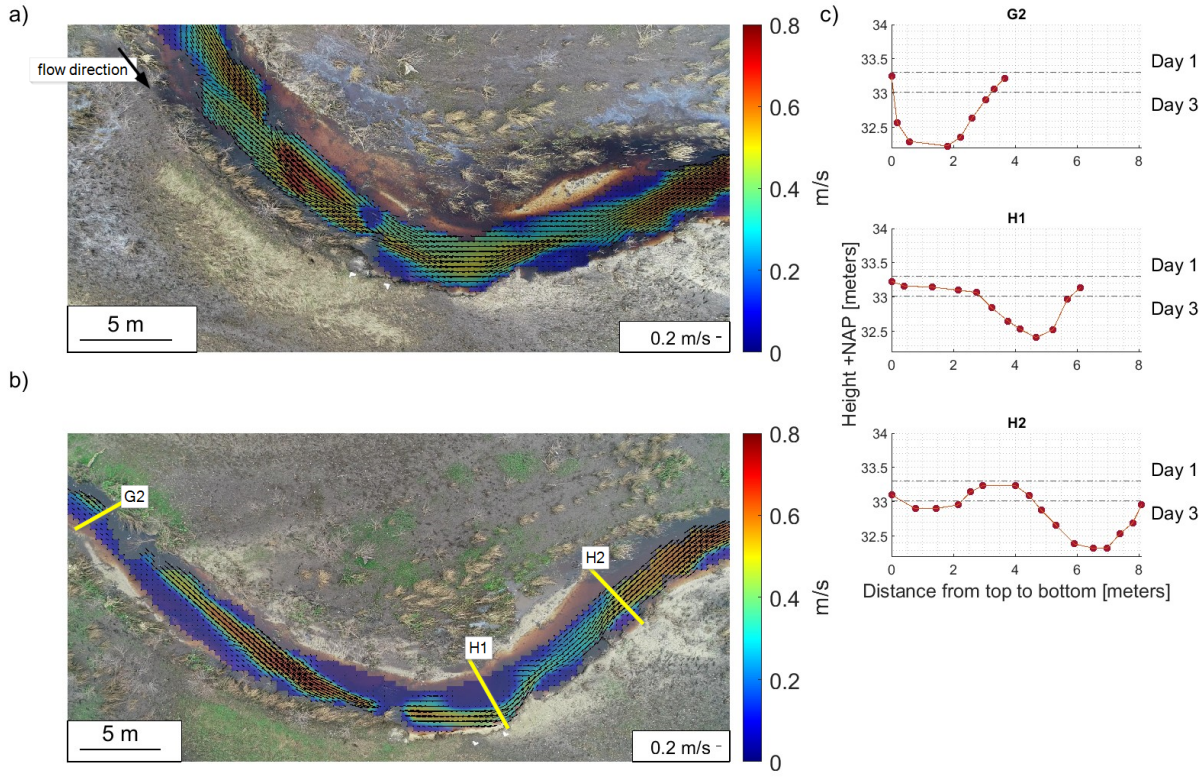

Figure 28: Surface flow velocities in bend 8 for day 1 (a) and day 3 (b), with the corresponding cross-sectional profiles displayed in (c), where the dots represent the RTK measurements. Bend characteristics are found in Appendix B and the size of the flow separation area in Appendix A

4.1.9 Bend 9

Figure 29 displays the surface flow velocities and cross-sections of the ninth bend. The ninth bend is a bend with a distinct point bar. During the third measurement day, this point bar was not fully inundated. Looking at the surface flow patterns, it is clear that the surface patterns differ between the first and third measurements. Furthermore, the maximum velocities differ 0.11 m/s, with the higher velocity on the first measurement day as expected. On both measurement days, the high velocity field is directed around the point bar, towards the outer bank, due to topographic steering. However, this direction is stronger and starts further upstream on the third measurement day compared to the first measurement day. In addition, it can be noticed that the reattachment point is earlier during the first measurement compared to the third measurement day. This is a similar pattern as observed in other bends.

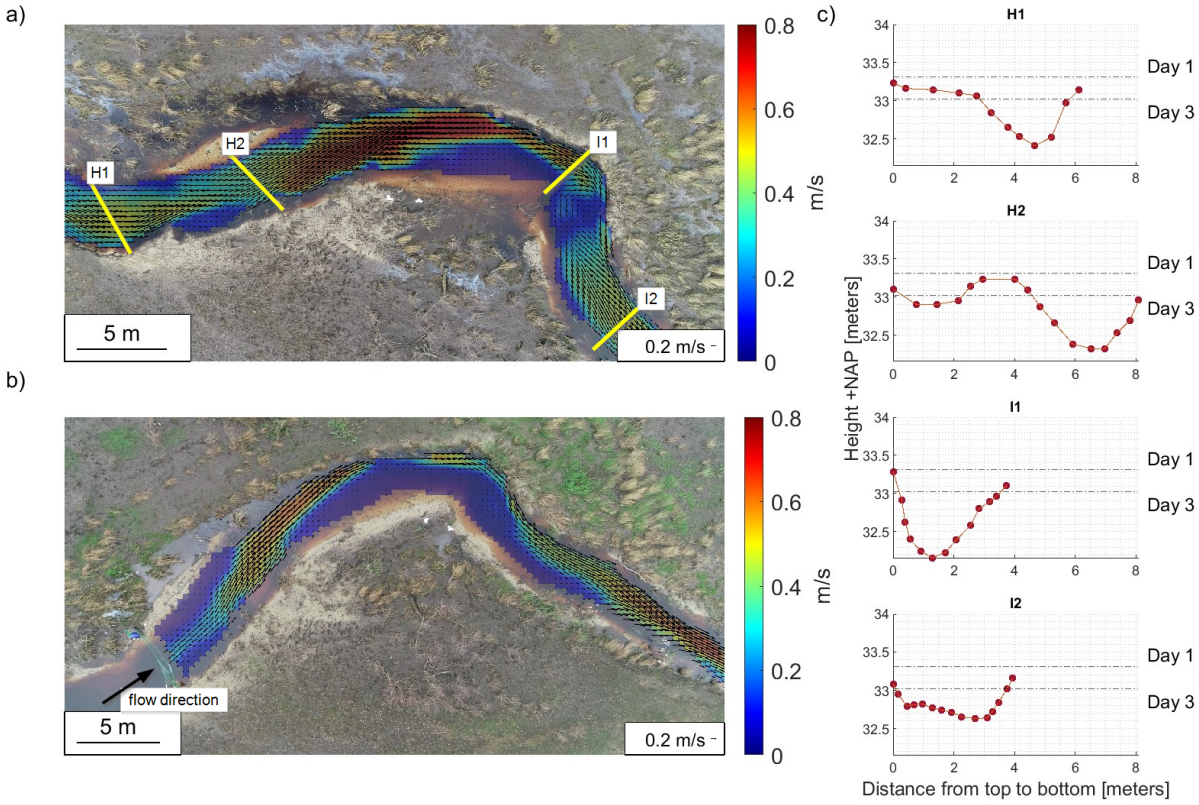

Figure 29: Surface flow velocities in bend 9 for day 1 (a) and day 3 (b), with the corresponding cross-sectional profiles displayed in (c), where the dots represent the RTK measurements. Bend characteristics are found in Appendix B and the size of the flow separation area in Appendix A

4.1.10 Bend 10

The last bend that will be considered is displayed in Figure 30. The flow pattern on the third day shows that the inner bend separation zone of bend 9 reaches all the way until the high velocity field impinges on the outer bend of bend 10. This impingement causes an inner bend separation area on both measurement days. However, it is more pronounced during the third measurement day. On the first measurement day, there is no distinct outer bend separation zone reaching from the previous bent. As mentioned before, there is an impingement of the high velocity field on the outer bend, causing inner bend flow separation. Cross-sections J1 and J2 show deepening of the channel in the middle and outer bend. It can be observed that the deepening of the channel has become more distinct after the apex of the bend. The measurement taken for cross-section J1 is a bit too short, such that it does not include the entire

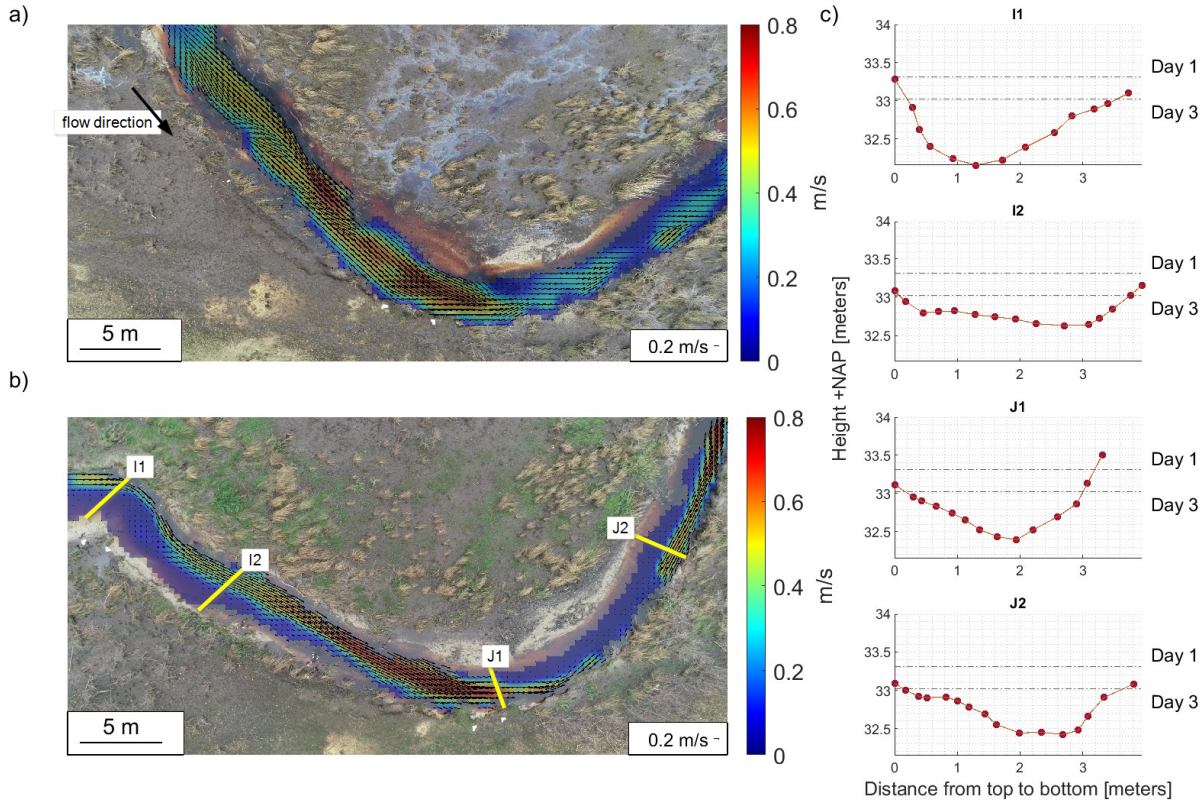

Figure 30: Surface flow velocities in bend 10 for day 1 (a) and day 3 (b), with the corresponding cross-sectional profiles displayed in (c), where the dots represent the RTK measurements. Bend characteristics are found in Appendix B and the size of the flow separation area in Appendix A

4.2 Correlation between bend characteristics and flow separation

In Figure 31, the sizes of the separation zones at the outer and the inner bend are plotted for measurement day 1 and day 3. Because an exact measurement of the area of the separation zones was sometimes difficult due to the exclusion of certain areas by the mask, a lower and an upper limit of the area has been used. The exact values of the upper and lower limits of the separation zones are also found in Appendix A. For a comparison with the, disregarded, values of the flow separation areas, the reader is referred to Appendix C. The total area of the inner and outer flow separation zones for both measurement days is also displayed. It can be seen that for both inner and outer bend flow separation, the areas are larger on the third measurement day, with lower flow depth. Looking at the uncertainty of the separation area, it is larger on day 1 for the inner bend separation and larger on day 3 for the outer bend separation.

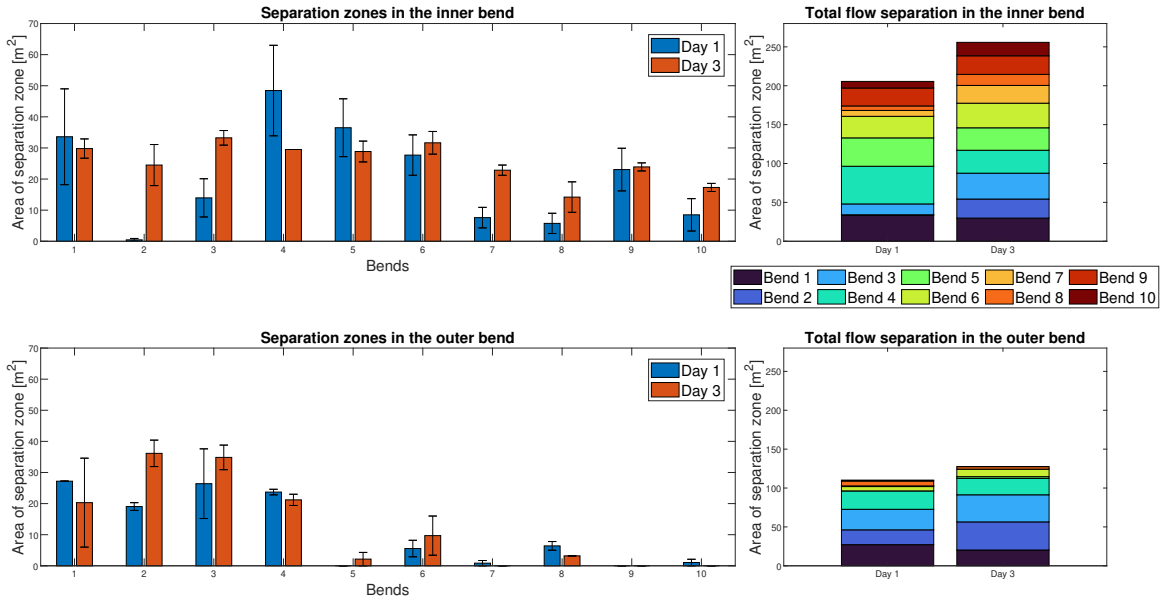

Figure 31: Areas of the flow separation zones for the inner and outer bend on day 1 and day 3. The bar graphs show the mean of the limits of the separation zones, and the error bars display the distance between the mean and the upper and lower limits of the separation zones.

Figure 32 shows the scatter plots of the remaining flow parameters: R/B ratio, radius, impingement angle and the increase in cross-sectional area, for both the inner and the outer bend. The exact values of each parameter can be found in Appendix B. The correlation coefficient has been calculated with the Pearson correlation coefficient (r):

$$r_{xy} = \frac{Cov(x,y)}{\sigma_x \sigma_y} \tag{10}$$

where $Cov(x,y)$ is the covariance between the variables and σ_x, σ_y denotes the standard deviations of x and y. In this case, x represents the area of the separation zone, either inner or outer bend and y represents the parameter for which the correlation coefficient is calculated, which can be found in Appendix B. The correlation coefficients are displayed in Table 10. The correlation coefficients have been calculated such that a value of +1 denotes a perfect positive correlation, -1 a perfect negative correlation and 0 no correlation.

The correlation between the separation areas and the R/B ratio is visualized in the upper row of Figure 32. For the inner bend separation, there appears to be a correlation to a certain extent for both measurement days. However, this correlation is larger for the first measurement day. The correlation coefficient for the inner bend on the first day is -0.57 and -0.39 for the third measurement day. For the outer bend separation zones, there is a small positive correlation for the third measurement day and a negative correlation on the first measurement day. Therefore it is expected that there is no strong correlation between the R/B ratio and the outer bend separation zones and a negative correlation with the inner bend separation zone, which is stronger at higher water levels.

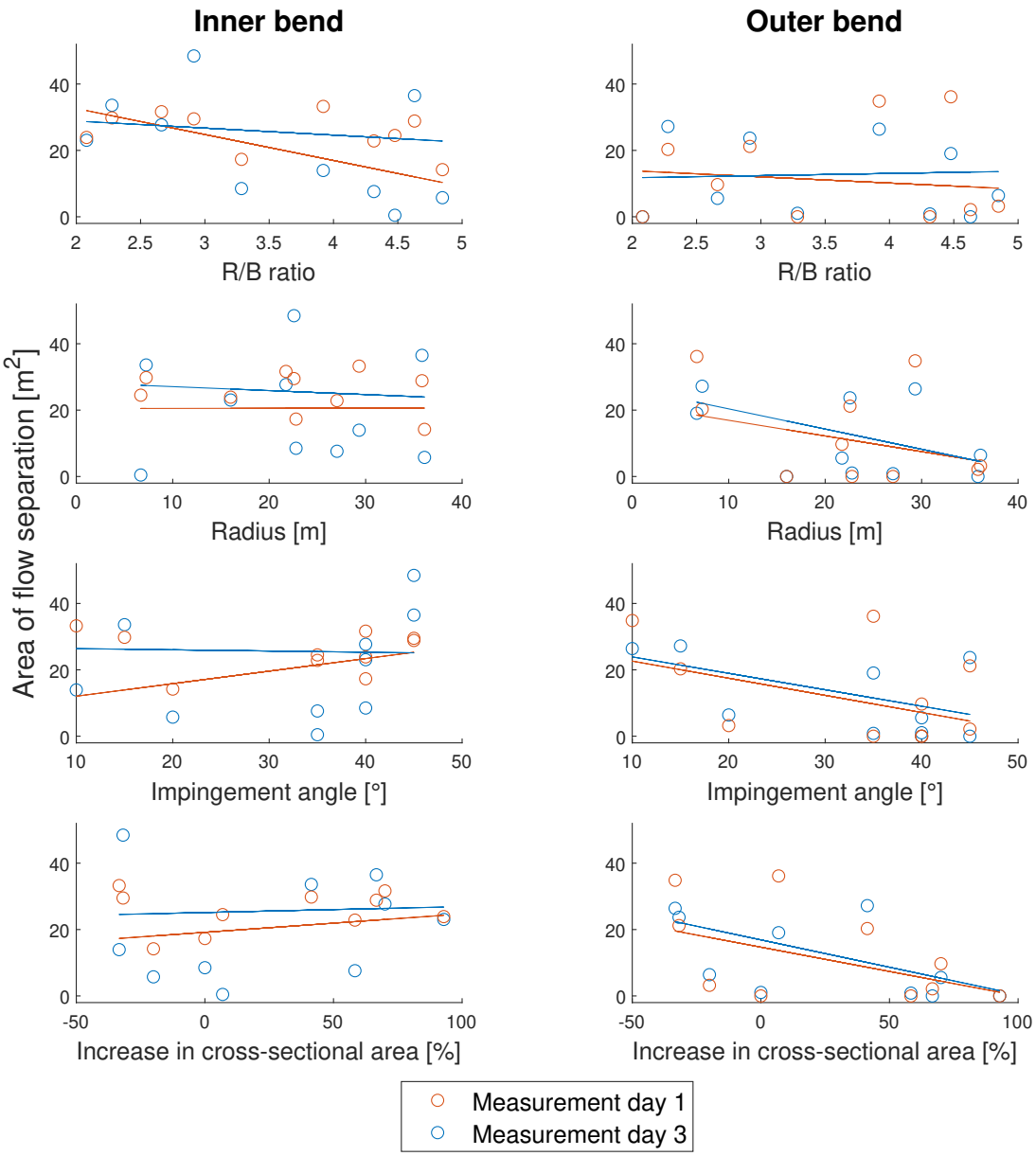

Figure 32: Scatter plots of R/B ratio, radius, impingement angle and increase in cross-sectional area for the inner and outer bend. Exact values of these parameters are found in Appendix B

In the row below, the correlation graph of the separation zones and the radius. In the left figure, displaying the relation with the inner bend separation zones, there is little to no correlation between the size of the inner bend separation zones and the radius of the bend. Small separation zones (< 10 m^2) are present for both small and large radii. For outer bend separation zones, there seems to be a negative correlation between the size of the separation zone and the radius. In other words, the size of the separation zone decreases with increasing radii. The correlation coefficient for the outer bend is on average -0.46 for the two measurement days combined.

Next, the correlation is shown for the impingement angle. The left figure shows that there is little to no correlation with the inner bend. In the figure on the right, there seems to be a negative correlation with the outer bend, such that the size of the separation area decreases with increasing impingement angle. The correlation at the outer bend is stronger on the first measurement day, with -0.63 compared to the third measurement day when it is -0.43.

Last, the correlation with the increase in cross-sectional area is tested. While the inner bend shows little to no correlation, the correlation with the outer bend separation area is the strongest of all parameters, with -0.62 on average.

In conclusion, the overall correlation is strongest for the increase in cross-sectional area and the area of the outer bend separation zone on both measurement days. The correlation between these parameters is negative, meaning that the size of the outer bend separation zone area decreases for an increase in cross-sectional area and becomes larger for a decrease in cross-sectional area. There is also some correlation between the impingement angle and the area of the outer bend separation zone. This relation is also negative and is more prevalent on the first measurement day. Next, it can be seen that there also is a negative correlation between the radius and the outer bend separation zone. So for a smaller radius, thus a high curvature, the separation zone is larger. Lastly, there is one parameter that correlates with the inner bend. This is the ratio between the radius and the width of the bend. This correlation is also negative and higher for the first measurement day.

Table 10: Correlation coefficient for the various parameters at the inner and outer bend on measurement day 1 and measurement day 3. The visual interpretation of cells is based on Table 11

	Inner bend separation zone, day 1	Inner bend separation zone, day 3	Outer bend separation zone, day 1	Outer bend separation zone, day 3
R/B	-0.57	-0.39	-0.18	0.05
R	0.00	-0.22	-0.46	-0.48
Impingement angle	0.34	-0.08	-0.63	-0.43
Increase in cross-sectional area	0.18	0.15	-0.65	-0.59

Table 11: Legend for colour interpretation. Source: Newcastle University, 2024

	Strong correlation (positive or negative) $1 > \|r\| \geq 0.8$
	Moderate correlation (positive or negative) $0.8 > \|r\| \geq 0.4$
	Weak correlation (positive or negative) $0.4 > \|r\| > 0$
	No correlation $r = 0$

5 Discussion

In this study, it was aimed to identify the influence of possible controlling factors of flow separation in the Glanerbeek, with the use of LSPIV and cross-sectional profiles. For the LSPIV analysis, no artificial seeding was used. Instead, natural surface tracers were created with a net to provide tracers for the LSPIV analysis. This is a new method that has not been used before, but that proved to be successful in displaying the general surface flow structure in the Glanerbeek. In this chapter, the observed flow structure in the Glanerbeek will be compared with findings from literature. This is followed by a description of the correlation analysis of the specific parameters in relation to literature. Next, the LSPIV's accuracy will be tested against the literature. In addition, the limitations of this research and recommendations for future research will be discussed.

5.1 Flow pattern

In Section 4.1, there were a few general observations that could be made. First of all, flow separation was more prevalent on the third measurement day compared to the first measurement day. This is plausibly caused by the difference in water level. This will be elucidated in Section 5.2.1. Also, from Table 16 and Figure 31, it can be seen that inner bend separation is present more often than outer bend separation. Inner bend separation occurred in almost every bend on both measurement days, while outer bend separation did not occur during at least one measurement day, on four out of ten bends. Parsons (2003) stated that while inner bend separation is more common, the areas are often smaller than the outer bend separation zones. In this case, the inner bend separation zones are indeed more apparent than the outer bend separation zones. However, the zones of the inner bend separation area is between 15.0 and 27.7 m^2 on average. The average of the outer bend separation zones is between 13.0 and 22.9 m^2. According to Blanckaert (2010), flow separation is more likely because downstream of the bend's apex, the flow velocities are lower which is favourable for the onset of inner bend flow separation zones, compared to the higher flow velocities upstream of the bend's apex. Hooke (2013) also found that flow separation was more prevalent in the inner bend. Hence, the findings are in agreement with Blanckaert (2010) and Hooke (2013) and partially with Parsons (2003).

The third observation that could be made was that in almost all locations, the main flow had the tendency to steer to the outer bend around the apex. This redirection appeared to be stronger on the third measurement day when the water levels and velocities were lower. This is likely caused by topographic steering. At higher discharges, the flow is more likely to be directed inward, while for lower discharges the flow will be forced more to the outer bank. Kasvi et al. (2013) found that the lower the discharge, the further downstream the flow is directed inward. Thus, these findings are corresponding with the findings of Kasvi et al. (2013). Moreover, the high velocity field was converging near the apex of most bends. This convergence was also found by Ferguson et al. (2003) and Vermeulen et al. (2015), who observed the high velocity field to converge asymmetrically, before the apex, in the direction of the outer bank until the width of the high velocity field was reduced considerably. Due to topographic steering, the flow collides with the outer bank. This is visible in bends 4, 5, 6 and 9. After this collision, there is a rise in water surface elevation, causing downwelling of the flow (Hodskinson and Ferguson, 1998) at the point of impingement causing the flow to impinge on the bed, which creates scour (Blanckaert, 2010). In each of these bends, the channel is indeed deeper around the locations of impingement, compared to the entry of the bend.

Due to the converging of the high velocity field due to a spiralling flow in the outer bend, and/or flow separation zones, it would be expected that this stream of reduced width should compensate in velocity due to the decreased area of flow. However, due to the increase in the cross-sectional area of the river caused by the outer bend pool, the high velocity field is rather decelerated. This change in velocity is most pronounced at the surface, where Ferguson et al. (2003) found the flow to decelerate with about 50% from the entry of the bend towards the apex. Downstream of the apex, the bend started to slowly accelerate again. On the other hand, the flow at the bed was fairly constant. In this study, the locations of maximum velocities were often found right before the point of impingement, which is contrary to the findings of Ferguson et al. (2003).

In the study in the Glanerbeek, no recirculation zones were observed over the point bars, even though the cross-sectional profiles showed that there were submerged point bars present. In literature, the presence of a point bar is often paired with an area of flow recirculation over the point bar, (Blanckaert, 2010; Blanckaert et al., 2013; Kasvi et al., 2013). A reason that could explain this lack of inner bend recirculation zones could be the inability of the tracers to access these zones within the time frame of the experiment. Another possible explanation would be that the flow over the point bar is too shallow, resulting in almost zero velocities at the inner bend.

The shallow flow over the inner bank can result in the onset of inner bank flow separation, but Hodskinson and Ferguson (1998) found that the point bar can also enhance outer bend flow separation. However, Parsons (2003) found a correlation between the inner bend separation zones and the point bar, but not with the outer bend separation zone. Since no specific prerequisites are known for the identification of a point bar in the field, it is difficult to determine in which of the bends a point bar is present. Especially since most bends have some sort of increase in the bed level at the inner bank. Moreover, a more detailed bathymetry of the bed should be known for the identification of the size of the point bar to find the correlation between the size of the point bar and the occurrence of flow separation zones.

5.1.1 Seeding

At each bend, the densities calculated in the ROI were plotted, these are visualized in Figure 19. It was found that the densities were in general higher during the third measurement day. This could have been caused by two people shaking the net on the third measurement day, against one person on the first measurement day. On both days, the upper and lower values of the density mostly did not show significant outliers, which means that the density was stable throughout the measurement day. In Pizarro et al. (2020a), densities between $0.4 \cdot 10^{-5}$ ppp and $1.0 \cdot 10^{-2}$ ppp were compared. It was found that densities lower than $1.0 \cdot 10^{-3}$ ppp result in a significant increase in error and therefore it is recommended to have a density of at least $1.0 \cdot 10^{-3}$ ppp for a LSPIV analysis. On day 1, four bends with densities lower than this threshold were found. During day 3, only one bend had a density below this threshold value. It should be noted that the densities are taken in a relatively small ROI, which is different for each river bend. Ideally, the densities should be monitored throughout the entire river stretch, or at the same location within each bend on the different measurement days. However, this was not done. Moreover, this density does not take into account the size of the particles, and therefore it cannot be converted to a density that is displayed in percentages, which would allow for a comparison with other LSPIV studies (e.g. Liu et al., 2021; Meselhe et al., 2004; Sharif, 2022)

5.1.2 Gaps in the surface velocity patterns

During the analysis of the results of the LSPIV calculations, it was noticeable that 'gaps' in the high velocity field occurred. These gaps are also shown in Figure 33. These occurred in multiple bends, at different places. This could be a low surface velocity at this location, but could also be caused by the LSPIV method. To test whether these gaps could have been caused by the absence of tracers in this area for the analysis period, a longer period of analysis was used, specifically 60 seconds. The results are shown in Figure 33. These figures show that the flow pattern throughout the bend remains the same with the increase in the analysis length. The only difference between the analysis of 30 and 60 seconds in Figure 33 is that the maximum velocity differs for both river bends. The difference is approximately 0.04 m/s, where the highest velocity is present at the video of 30 seconds for bend 3 and for the video of 15 seconds for bend 10. When looking at the density values, it can also be seen that the videos with the most gaps do not have significantly lower amounts of densities. Moreover, the densities in these bends are quite stable over the monitoring period, so a fluctuating seed could not have been the cause for the gaps in the analysis.

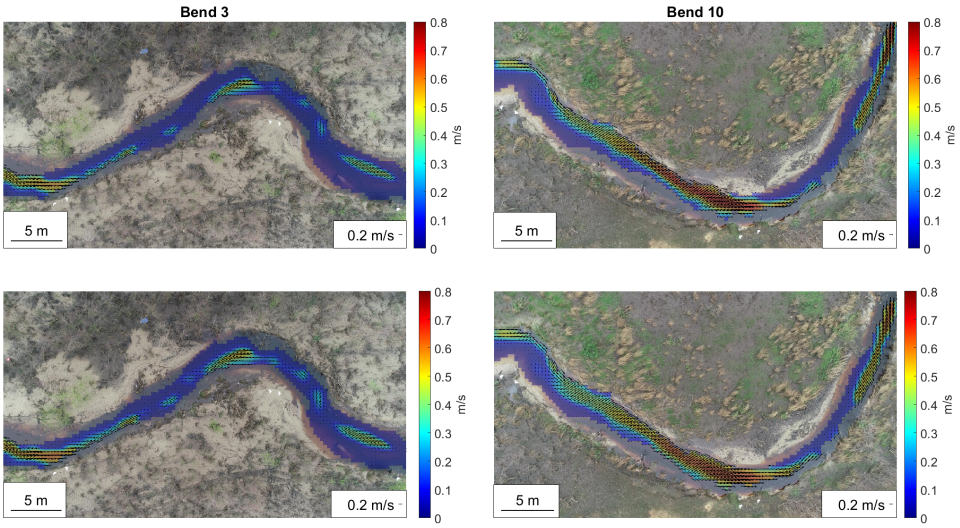

Figure 33: Difference between LSPIV analysis of 30 (top figures) and 60 seconds (bottom figures) in bend 3 and bend 10. The flow direction is from left to right. The reference vector displays the maximum velocity.

In conclusion, the gaps in the high velocity field are most likely not caused by the absence of particles in this part of the field. Therefore, a longer analysis time would not have contributed to a better analysis. When examining the videos, it can be seen that there are particles present at the location of the gaps. Another hypothesis would be that the gaps are caused by the illumination at these locations. For example, in bend 3, some of the gaps are located in the shadow of the vegetation. However, this is not the case at each gap location. Therefore, the question remains what the explanation behind these gaps is.

5.2 Parameter comparison

In this section, the correlation between the parameters and the area of flow separation is discussed. The correlation graphs are found in Figure 31 and 32. The correlation is observed graphically and tested with the correlation coefficient for linear correlation (Table 10). It was chosen to focus solely on a linear relation because the field study of Parsons (2003) focused on a linear relation between possible controlling factors and the size of the areas of flow separation, and because of the simplicity of a linear relation. However, it can be expected that the relations between the controlling factors and flow separation are not necessarily linear. For example, Blanckaert (2010) found in an experimental study that a nonlinear interaction between sediment transport and the flow, resulted in an equilibrium situation with flow separation. Moreover, Blanckaert and De Vriend (2010) showed that the hydrodynamics in meander flows can be best described with a nonlinear model, because of the mutual interactions between various hydrodynamic processes.

It is important to realize that these relations do not describe a causal relation. Cause and effect can be partly deducted from theoretical knowledge, but the question remains whether flow separation is a result of these parameters or whether the parameters are caused by the hydrodynamics of the flow separation zones. At the same time, a lack of correlation can be caused by multiple factors, such as a small sample size of only ten bends in the same stream, which can result in a lack of correlation or a misjudged correlation.

5.2.1 Relation with flow depth

The flow depth is an interesting parameter because it is the only parameter which can be used to compare the flow pattern at the same bend. However, for more extensive research, multiple measurement days are required with varying water levels. The water level of the excluded data, from measurement day 2, was in between the water level of measurement 1 and measurement 3. Although, including these measurements could have been interesting for the relation of flow separation with the flow depth, it would have been more valuable if the water level was lower or higher than measurement day 1 or 3. The flow depth used in this analysis is not specified along the width of the channel but is rather taken from the water level on both days, representing a higher and lower flow depth in the river on the different days.

In Chapter 4, it was found that the area of flow separation was larger with lower flow depth, for both the inner and the outer bend. The decrease in water depth is accompanied by a decrease in flow velocities in this study, which leads to lower inertia. In bend 1, the higher inertia on day 1 leads to an increased separation zone on day 1 compared to day 3. Contrarily, the zone of flow separation decreases with decreasing water depth in bend 2, which is possibly also caused by a difference in inertia. Thus, it seems that an increase in inertia can both favour and prevent flow separation, dependent on the characteristics of the river bend and the inflow conditions.

In general, theoretical knowledge on flow separation describes that flow separation increases with increasing flow depth, for example, in Equation 3, which is based on the numerical study of Bo and Ralston (2020). Contrarily, observing the flow structure in the field in the Glanerbeek, it was found that flow separation, generally, increases with decreasing flow depth, as the area of flow separation zones was higher for the third measurement day, when the water depth was lower. This can be seen in Figure 31. The increase in flow separation area was strongest for the inner bend separation zones. This could have been caused by a shallow flow over the point bar at the higher water level, resulting in stagnant flow over the point bar, which is considered as flow separation based on the surface flow patterns.

Kasvi et al. (2013) stated that the most important parameter for flow separation over the point bar is the flow depth over the point bar, which could explain why the inner bend separation zones were larger for the third measurement day. This does not necessarily mean that the flow separation zones are always larger for lower water levels, as Kasvi et al. (2013) found that the separation zones were larger for higher discharges, when studying meander point bars in a field study of the Pulmanki river in Finland. In the Pulmanki river, at low discharge, the point bar was mostly exposed and the flow depth over the inundated section of the point bar was high. At high discharges, the whole point bar was inundated and the flow depth was lower over the part of the point bar where flow separation became present. Therefore, the flow depth over this part of the point bar was lower, allowing for flow recirculation. Hence, the flow depth over the point bar is the controlling factor of the inner bend separation zone rather than the general water level in the river (Kasvi et al., 2013). In addition, in a laboratory study, Kleinhans et al. (2010) found that the flow patterns were not influenced by differences in water level. A possible reason for the differences in flow separation area might be the low flow depth over the point bar causing stagnant flow, similar to the study of Kasvi et al. (2013), rather than the general water level in the Glanerbeek. For future research, it would be interesting to see what the influence of the flow depth within the flow separation zones is and if there is a significant difference between the bends, and/or a significant difference between the flow depth at inner and outer bend separation zones.

5.2.2 Relation with radius

In Figure 32 and Table 10, it can be seen that the correlation with the radius is mainly prevalent for outer bend separation, with a correlation coefficient of -0.46 for day 1 and -0.48 for day 3. Thus, the size of the separation zone increased for decreasing radius, and thus increasing curvature. Kim et al. (2020) also found that increased curvature does not only determine the onset of flow separation but also the size, as the size of the separation zones increases with increasing curvature (Kim et al., 2020). In the study of Kim et al. (2020), flow separation was limited to outer bank separation. Therefore, the results are in agreement with this modelling study. In a laboratory setting, Blanckaert (2010) found that, when a point bar is present, topographic steering increases with increasing curvature, resulting in a shallow flow over the point bar. This shallow flow results in flow recirculation in the inner bend. This relation was not found in this study.

Calculating the radius in field studies is difficult, as the curvature varies throughout the bend and the shape of the bend is not a perfect arc, as it is in laboratory studies (Parsons, 2003). The same holds for the width of the stream. Determining the overall radius of the river bend depends strongly on the definition of the starting and end points of the bend. To increase the accuracy of the calculated radii, a circle was plotted over the apex of the bend to validate the radius calculated by the script. Evidently, the accuracy of the plotted circle is also dependent on the definition of the starting and end point of the curvature, which makes this approach not flawless. It was chosen to use the same approach in each of the river bends, so the radii could be compared in their relation to the other bends.

5.2.3 Relation with R/B ratio

The relation with the R/B ratio is only present for the inner bend separation zone and is -0.57 on day 1 and -0.39 on day 3. Thus, for smaller R/B ratios, the separation zones are larger in the inner bend. The influence of the R/B ratio is one of the most studied parameters with regard to flow separation. In the literature, flow separation is often present for $R/B < 2$ (Bagnold, 1960; Finotello et al., 2020; Nanson, 2010)

or R/B < 3 (Bagnold, 1960; Hickin and Nanson, 1975). In these studies, the separation zones are mostly inner bend separation zones. In this study, the R/B ratios ranged from 2.1 to 4.8. Inner bend separation zones were present for almost every bend, but the size of the separation zones increased slightly with decreasing R/B ratios. This increase in separation zone is in line with Equation 3, which describes the advection-friction ratio K_r for inner bend flow separation, which is dependent on the water depth and the R/B ratio. This equation describes that K_r increases for decreasing R/B ratios. Since the study of Bo and Ralston (2020) was limited to inner bend flow separation, no information on the influence of the R/B ratio on outer bend separation is available. In theoretical papers regarding flow separation, it is stated that a R/B ratio lower than 3 is required for the onset of flow separation. This is not in line with the study of the Glanerbeek, where inner bend flow separation occurred for each R/B ratio.

Blanckaert (2010) developed a requirement for the onset of outer bend flow separation:

$$\frac{R_{min}}{B} < \sqrt{\frac{1}{2C_f}\frac{h}{B}} \tag{11}$$

While this requirement cannot directly be tested because of the lack of information on C_f, the requirement states that flow separation is favoured in smooth, narrow and high curvature bends and that there is no general threshold of the R/B ratio for the onset of flow separation, but rather that it is dependent on the characteristics of the river bend. As mentioned in section 5.2.2, calculating the exact radius and width of the bend is difficult in field experiments. Therefore, it is to be expected that the onset of flow separation in the river bends is not exactly at R/B < 2 or < 3. The finding that there is a negative correlation between the R/B ratio and the inner bend separation zone is more important, which is in line with Blanckaert (2010). Contrary to Blanckaert (2010), in this study (Glanerbeek), no correlation between the R/B ratio and the outer bend flow separation was found.

5.2.4 Relation with impingement angle

In bend 8, the difference between the first and third measurement day could be caused by the difference in inflow conditions at the entry of this bend. The influence of the inflow conditions was also demonstrated in numerical studies by Ferguson et al. (2003) and Hodskinson and Ferguson (1998) and in a field study executed by Nanson (2010). Moreover, the inflow conditions can also be linked to the impingement angle.

The impingement angle showed a negative correlation with the outer bend separation zone, which was -0.63 on day 1 and -0.43 on day 3. A weak correlation was present with the inner bend separation zone on the first day (0.34). However, this correlation was not present on the third day, where it was -0.08. Based on these results, it is expected that there is only a correlation with the outer bend separation zones.

The impingement angle is one of the parameters that correlates most strongly with outer bend separation. This strong correlation was also found by Parsons (2003), for both inner and outer bend separation. However, in the case of Parsons (2003), the correlation was positive, meaning that the size of the separation zones increased with increasing impingement angle. It is unsure where the differences in these findings are coming from, as the same method for the calculation of the impingement angle was used and the observed flow separation area was also taken from the surface flow. However, with this estimation, it would still be expected that the correlation is in the same direction as in the literature.

5.2.5 Relation with increase in cross-sectional area

The correlation with the increase in cross-sectional area was found only for outer bend separation zones. The relation found was negative, with a correlation factor of -0.65 for day 1 and -0.59 for day 3, making it the strongest correlation of all characteristics. The negative correlation implies that the increase in cross-sectional area results in a decrease of the outer bend separation zone. This is contrary to the findings of Vermeulen et al. (2015), who stated that the increase of cross-sectional area results in an increase in the size of the separation zone, both at the inner bend and at the outer bend. The cross-sectional area in Vermeulen et al. (2015) became three times larger. In the Glanerbeek, the maximum increase in cross-sectional area was 93%, so it was not even two times larger than at the entry of the bend. However, it would be expected that this would lead to a less strong correlation or even no correlation, but it cannot explain why the flow separation area would decrease instead of increase.

Blanckaert et al. (2013) tested the flow separation pattern in a laboratory flume for the difference between constant-width and widening open-channel bends. It was found that for bends where the channel was widened at the apex of the bend but the bed was immobile, there was a weakly circulating outer-bank separation zone which hardly influenced the main flow. For mobile beds, it was found that the widening of the channel caused this separation zone to disappear eventually, as the morphology of the bed developed. Moreover, they found that the widening of the channel favours the onset of flow separation at both the inner and the outer bank. Due to these findings of Blanckaert et al. (2013), it was assumed that an increased width at the bend's apex was an important parameter in flow separation induced by an increase in cross-sectional area. Therefore, the difference between the cross-sectional area at the entry and the apex of the bend was calculated. However, Blanckaert (2010) found that the maximum increase in cross-sectional area is situated just downstream of the entrance of the bend. Moreover, increases in the cross-sectional area due to scour are usually found upstream of the point of highest curvature (Vermeulen et al., 2015). Hence, the cross-sectional area at the bend's apex could have been already decreasing with respect to the point of maximum cross-sectional area, assuming the location of maximum curvature is found slightly upstream of the bend's apex, as suggested by Blanckaert (2010). As a result, the reverse correlation might be attributed to the methodology. It is recommended to have more detailed information on the cross-sectional areas throughout the bends for a thorough analysis of the influence of the increase in cross-sectional area on the flow separation zones.

5.3 Accuracy assessment

Looking at Table 4 and 6, it can be seen that most values of the NMBE and NMRSE are within the range of +-6-28% and 10-40% respectively. However, there are some outliers (where the NRMSE is approximately 10 times larger than the other values) which increase the average values of the NMBE and the NRMSE significantly. These outliers are likely caused by measurement errors either during the LSPIV analysis or the float methods.

While focusing on the accuracy of the field study, it is important to put the error metrics in perspective of other studies found in the literature. For example, in a study of the Dinkel, a small river close to the Glanerbeek, Sharif (2022) found values of a NRMSE between 5.0 and 8.8%, with an average of 6.6%. Similar to this research, the error metrics in the study of Sharif (2022) were calculated with the use of the float method. In the Glanerbeek, the NRMSE was between 8% and 75%, with an average of 22%. The NMBE in Sharif (2022) was between 0.5% and 4.9%, which indicates that the LSPIV analysis tended to underestimate the velocities in the river as well. However, when looking at the results in Table 4 and Table 6, it can be seen that the LSPIV analysis not only underestimates the velocities but also sometimes overestimates the velocities. At the same time, the NMBE is of a higher order, as it ranges from -22% to +283%. It should be noted that the analysis of Sharif (2022) was executed near a weir, which caused a lot of foam which could be traced. Moreover, the analysis was executed in a straight river section, which results in more uniform surface velocities.

In Clear Creek in Iowa, a creek with an average discharge of 0.2 m^3/s, Bradley et al. (2002), tested PIV techniques in an artificially seeded flow. Contrary to Sharif (2022), the river sections were not necessarily straight in this research. The camera was mounted on a bridge and the reference velocities are measured with a current meter. The RMSE that was found was 0.032 m/s, with the maximum value of the velocity of 0.22 m/s. From the data presented in the paper, the NRMSE cannot be calculated. During the research in the Glanerbeek, the average RMSE was 0.13 m/s on measurement day 1 and 0.12 m/s on day 3. The maximum velocity measured with the float method in the Glanerbeek was 0.64 m/s. In conclusion, for the Glanerbeek, with a maximum velocity of approximately three times as large, the RMSE is approximately four times larger. In other words, the normalized value of the RMSE in the Clear Creek would be slightly lower compared to the study in the Glanerbeek.

In a study of Pizarro et al. (2020a), three different case studies in Italy were analysed. The mean surface velocities were between 0.38 - 0.82 m/s, which is comparable to this study. Additionally, a case study in the UK was used for validation purposes. At three out of four locations, an Unmanned Aerial System (UAS) was used, while in the other location, the imaging system was fixed on a bridge. Artificial seeding was applied in this study and the reference velocities were measured with a current meter, allowing for more accurate results compared to the float method. The error metric used for this study was the Mean Absolute Percentage Error, which is calculated as:

$$MAPE = \frac{1}{n} \sum \frac{|U_{Ci} - U_{Ri}|}{U_{Ri}} * 100 \tag{12}$$

In the study of Pizarro et al. (2020a), the MAPE ranged from 9.4% to 14.3%. Calculating the same error metric for this study, the MAPE values are 22.6% for both measurement day 1 and day 3.

Pearce et al. (2020) researched the River Kolubara, in central Serbia. During this study, the effectiveness of LSPIV was tested at low flows with high seeding densities, using a UAS. The seeding was done with artificial tracers and the average surface velocities were 0.12 - 0.14 m/s. It was found that the LSPIV tended to underestimate the surface flow, which is in line with this research. It was found that the velocities computed with LSPIV were deviating 0.05 m/s from the reference velocities, which were taken with Acoustic Doppler Current Profiler (ADCP) measurements. In this research, the computed velocities deviated 0.09 m/s on measurement day 1, and 0.10 m/s on measurement day 3. While the average surface velocities of the Glanerbeek are unknown, it is expected that they are higher than the Kolubara, and that the error might be in the same range as the study in the Kolubara.

In Ilinois, Lewis and Rhoads (2018) studied two river confluences with an UAS. Next, Acoustic Doppler Velocimetry (ADV) measurements were used to test the accuracy of the LSPIV analysis. Artificial seeding was used. It was found that the LSPIV velocities were mostly within 5% of the ADV measurements. For these rivers, this implied that the computed velocities were in the order of cm/s of the reference velocities, with velocities in the rivers up to 0.35 m/s. In South Korea, Kim et al. (2004) studied the Neungwon and Gonjiam streams to test the accuracy of LSPIV. Here it was found that the maximum difference between the

reference velocities was 8%, where the reference velocities were obtained by a 3D electromagnetic current meter and electron-wave surface meter. It is not clear if additional seeding was applied in these streams. As mentioned before, in the research in the Glanerbeek, the computed velocities were on average 22.6% from the reference velocities.

Creëlle et al. (2018) tested the influence of vegetation on the accuracy of LSPIV in the Zwarte Nete, Belgium. This was done by monthly measuring the stream surface velocities with the application of LSPIV. It was found that the LSPIV is most reliable in winter. The accuracy of LSPIV was tested by testing the computed velocities with reference velocities obtained by an electromagnetic current meter (ECM). Next, the discrepancies were calculated as:

$$d = \frac{|U_c - U_{ECM}|}{|U_{ECM}|} * 100 \tag{13}$$

Where d is the discrepancy, U_{ECM} is the velocity measured by the ECM. The discrepancies were between 5.9% and 40.1%, with the highest discrepancies in the summer. In winter, the same season as the field study in the Glanerbeek, the discrepancies were between 5.9% and 15.9%, with an average discrepancy of 9.8%. In the Glanerbeek, the discrepancies were between 3.2 % and 73.9 %, with an average of 22.6%.

In a flume study, Kim (2006) found that the difference between these errors is mainly caused by the cross-sectional location of the velocity measurements. More specifically, the illumination and seeding are important factors in the errors with LSPIV. Furthermore, Creëlle et al. (2018) observed higher discrepancies for points which were closely located to the river banks. This could cause some of the location-specific trends in errors as discussed in Chapter 4. Muste et al. (2008) showed that the error is also dependent on the methodology with which the reference velocity is obtained, as at the same location, the difference in velocities was up to 10% when tested against an ADV (Muste, 2004) and 16% when tested against a mechanical current meter (Bradley et al., 2002).

In this section, the accuracy of the LSPIV measurements has been compared with regard to other studies. Table 12 provides an overview of these findings. It can be concluded that the accuracy of the measurements in this study is lower than in other studies. However, since this is one of the first studies using natural surface tracers generated by a net and the optimization of this process was not the main goal of the research, this method seems promising. Moreover, the influence of the outliers which were present in this study (which were up to 10 times larger than the average value) should not be disregarded. It is recommended to identify the factors contributing to the larger errors, especially at the outliers. Factors could for example be the location at which the reference velocities are measured (Creëlle et al., 2018; Kim, 2006) or the method for obtaining the reference velocity (Muste et al., 2008). Since most measurements in the literature were executed in a (somewhat) straight river section, it would be interesting to test this method for generating natural surface tracers in a straight river section to exclude the influence of the bend on the error metric. However, this is not within the scope of this research and thus will be a recommendation for future research.

Table 12: Accuracy comparison of LSPIV in the Glanerbeek with studies from literature

Authors	River	Seeding	Type of river section	Reference method	Error metric	Value	Value this study
Sharif (2022)	Dinkel	Natural	Straight	Float method	NRMSE NMBE	5.0 - 8.8 % 0.5 - 4.9%	8%- 75% -22 - +283%
Bradley et al. (2002)	Clear Creek	Artificial	Non-straight	Current meter	RMSE	0.032 m/s Max velocity: 0.22 m/s	0.12-0.13 m/s Max velocity: 0.64 m/s
Pizarro et al. (2020a)	Brenta Noce Bradano Arrow	Artificial	Straight Straight Straight Non-straight	Current meter	MAPE	9.4 - 14.3%	22.6 %
Pearce et al. (2020)	Kolubara	Artificial	Straight	ADCP	Deviation	0.05 m/s	0.09 - 0.10 m/s
Lewis and Rhoads (2018)	Saline Ditch & Kaskaskia River	Artificial	Confluence	ADV	Deviation	5%	22.6%
Kim et al. (2004)	Neungwon & Gonjiam stream	?	?	electromagnetic current meter and electron-wave surface meter	?	8%	22.6%
Creëlle et al. (2018)	Zwarte Nete	Artificial	Non-straight	Electromagnetic current meter	Discrepancy	5.9 - 15.9 %	3.2 - 73.9%

5.4 Limitations

Although flow separation is a phenomenon that occurs in three dimensions in a river, this research was only focused on the surface flow patterns. At the surface, the flow separation zones are larger compared to the bed, especially at the apex (Ferguson et al., 2003). Moreover, the flow can have a different direction at the surface and at the bed (Ferguson et al., 2003). Therefore, focusing only on the surface flow velocities does not capture all the flow processes involved in the occurrence of flow separation and the observed flow structure. Adding to this, LSPIV can only capture the flow that can be observed by eye (Pearce et al., 2020). Hence, using the float method as a method for reference velocities increases this bias. Moreover, if the generation of the tracers influences the surface flow pattern, for example by standing in the river, these tracers can be correctly traced by the LSPIV and they are traced in a similar way by the float method. In that way, the reference method also measures the disturbed pattern. Therefore, this does not have to result in an increase in error, while it could affect the flow pattern in the stream. A better way to obtain the reference velocity would be by using a method that uses a different mechanism to compare the velocities generated by the LSPIV, such as an ECM or ADCP. Nevertheless, these methodologies have their own limits, for example, that they are intrusive in the flow.

In this research, the secondary flow has not been considered because no velocity measurements could be done over the depth of the flow. The influence of the secondary circulation on flow separation in beds with a point bar and pool is questionable. Blanckaert (2015) found that the influence of the secondary circulation on flow separation is significant in flat-bed experiments, but is insignificant for inner bend separation zones in non-flat beds as the circulation cell is mostly present in the outer bend pool. Ferguson et al. (2003) observed secondary flow at the first part of the bends. While the strength of the secondary flow was favoured by the convergence of the high velocity field towards the outer bend, the effect on flow separation was reduced by the increase of flow depth at the outer bend pool. Moreover, the plunging on the outer bank was stronger than the upwelling in the middle of the stream (Ferguson et al., 2003). In a bend with deep scour, Vermeulen et al. (2015) observed a secondary flow cell in the bend but it was located near the bed. Therefore, it could be possible that the effect of the secondary flow cell on the inner bend flow separation zone is dependent on the depth of the outer bend pool. However, in creeks with no point bar, Nanson (2010) found that the size of the secondary flow decreases with increasing velocity. Moreover, the secondary flow was absent in sharp curves. Compared to the study of Nanson (2010), the bends in the Glanerbeek are not that tight, which is why it would be expected that the secondary flow would be present. The secondary flow cell creates an upward and outward force at the inner bend, favouring inner bend flow separation by directing flow away from the inner bend. Moreover, it strengthens the shear layer between the inward-directed pressure gradient and the outward-directed secondary circulation cell at the upper part of the water column. Since the secondary flow decreases with increasing velocities, outer bend flow separation would be favoured on the third measurement day. This could explain the increased flow separation on the third measurement day. It would be interesting to study the difference in flow separation zones for varying pool depths.

For the classification of flow separation zones, no objective guidelines have been used, other than a subjective classification of whether something is a 'typical' flow separation zone. Parsons (2003) excluded small-scale separation zones, with a width < 1/8 of the channel width, in their analysis because these zones could have been caused by collapsed bank material or irregularities in the river bank. While this study did not use specific classifications, zones caused by bank irregularities or collapsed materials have been excluded from the analysis.

Another aspect of the research is the cross-sectional profiles taken with the RTK. These cross-sections provided information about the bed profile. However, these measurements would have been more valuable if they were taken at more locations throughout the river. Ideally, a 3D bed profile of this section of the Glanerbeek would have been included, but this was too time-intensive for this research. Now, the cross-sections were mainly used for the identification of whether an increase in cross-sectional profile was present throughout the bend. However, it would have also been interesting to see whether changes in the bed profile were present at the location of the onset of flow separation, at the maximum width of flow separation and at the reattachment point of the separation zones. Moreover, the RTK measurements were taken with an RTK pole with a sharp tip point that was sinking into the soil. All the measurements were corrected by adding the length of the tip to the measurements. However, the amount of error due to the tip is not equal at each location. Therefore, this could have resulted in some small measurement errors (between 0 and 82 mm).

The water levels were also measured with the RTK. However, the locations of these RTK measurements differed approximately 90 meters between measurement day 1 and measurement day 3. Therefore, it could be that some deviation between the water levels was caused by this. However, since the discharge measurements are also available for the Glanerbeek and a difference in the water levels can also be perceived on the aerial pictures, the observation that the water level was higher on the first measurement than on the third measurement day can be confidently made.

The sensitivity analysis was performed with a video from an earlier measurement day. The reason behind this was to check the flying height and the performance of the LSPIV before the measurements. However, it would have been better if the sensitivity analysis was performed with measurements that were included in the research because the performance of LSPIV is dependent on specific illumination, wind ripples on the water surface, the amount of movement of the drone due to the wind, etcetera. Therefore, performing the sensitivity analysis on the footage used for the analysis could have increased the accuracy of the results. On the other hand, using footage from previous field visits allowed for an earlier start of the analysis of the results and the ability to analyse the results before the next field visit. Thus, it remains a trade-off on which method could have been used. Another aspect of the sensitivity analysis that could have been improved, was that currently only one video has been used for the execution of the sensitivity analysis. Therefore, some of the settings chosen were not only time-specific but could also have been site-specific. This would also increase the time required for the sensitivity analysis, but analysis of the results between the measurement days would have been possible. In addition, the question remains, for both the time-specific and site-specific case whether this increased workload would have resulted in a different outcome of the sensitivity analysis, as the results of the sampling frequency and the interrogation area were convincing even with the use of one video. Certainly, adding more locations and performing the sensitivity analysis on the footage from the measurement days would have made the analysis more robust.

The SDI is used as a metric to select the frames that contain the most information for the LSPIV analysis. For this SDI, a ROI has to be selected. Where the ROI is placed matters for the amount of tracers visible in the SDI. Now, it was chosen to select the ROI as large as possible and have approximately the same size of the ROI for each video. However, the results could have been further improved when the ROI was selected in a low seeding area, such that the SDI could act as a method to ensure sufficient seeding in the low-density areas of the river bends. Moreover, the SDI could have been used as a metric to compare the quality of the seeding in this research to the error metrics.

The areas with low density are a difficult problem in the LSPIV analysis. When there are no seedings present that LSPIV can use to approximate the velocities in a certain area, LSPIV interpolates the velocities in these areas with the surrounding velocities. Therefore, the velocity in the area of low velocities is likely close to zero and not caused by low densities, as otherwise the velocities would have been interpolated with moving tracers and would not result in zero velocities. Due to the method used for creating the tracers, the tracers are mainly focused in the high velocity zones of the stream. This is because the tracers are generated more easily when flow of high velocity passes through the net. However, when artificial tracers would have been used, most tracers would also be directed to the area of high velocity flow.

The video length was kept long to increase the probability of having tracers in each part of the stream. However, this also increases the probability of environmental disturbances (Pumo et al., 2021). Moreover, Sharif (2022) and Pumo et al. (2021) found that the accuracy was steady from a duration of 4 and 5 seconds respectively. In retrospect, it would have been better to choose a shorter duration of video length and ensure sufficient seeding density, by using the SDI for the selection of the best frames. Additionally, this would have significantly decreased the computational time.

In Chapter 1, the horizontal shear was mentioned as a factor that could prevent the onset of flow separation even though an adverse pressure gradient is present. In this research, it was assumed that the shear would be similar on the first and third measurement days. However, as the field experiment was executed at the end of the winter, there could have been vegetation growth towards the third measurement day, resulting in increased shear caused by the vegetation. This should have resulted in a reduced onset of flow separation. In this research, there is no method to exclude the difference in vegetation on the onset and size of the separation zones, as was done in Creëlle et al. (2018). Including these seasonal differences in vegetation, it would be interesting for future research.

5.5 Recommendations for future research

In this Discussion Section, multiple recommendations have been mentioned. In this section, these recommendations will be summarized. First of all, it is recommended to further research the methodology for generating the seeds for the LSPIV analysis and possible influences on the error. As this method for generating tracers has been used for the first time, it is expected that with some fine-tuning, the method has the potential to be used as an eco-friendly alternative to adding tracers in low-seeding streams. Moreover, as most LSPIV analyses found in the literature were executed in straight river sections, it is recommended to fine-tune the method in a straight river section. This also allows for a better insight into the parameters affecting the level of error. Additionally, it is recommended to further research the effect of the seeding density and the effectivity of the SDI on the accuracy of LSPIV in field studies. Moreover, it would be recommended to calculate the densities and the values of the SDI at the locations where the reference velocities were taken, to gain insight into the relation between the density, SDI and the error.

Next, it is recommended to execute this research on multiple days, for a better understanding of the effects of the water depth on the flow separation areas. This could also give insight into the effects of the vegetation on the flow pattern in this stream. More extensive research could also be done by increasing the amount of cross-sectional profiles. This could give insight into the change in bathymetry at the location where the flow separation onsets and at the reattachment point.

To increase the certainty in the accuracy assessment, it is recommended to use a different method for taking the reference velocities, that uses a different approach in obtaining the reference velocities than the LSPIV analysis. Predominantly, this sensitivity analysis shows that there are other factors contributing to the NRMSE than solely the tracer-generating method and the distance from the net, which are likely more influential than the aforementioned factors. Therefore, for a thorough comprehension of the factors contributing to the NRMSE throughout this method, it is recommended to perform a more extensive sensitivity analysis, covering all factors that could be of influence to the errors within this method, such as comparing the influence of the location where the reference velocities are taken and the influence of the net on the surface flow pattern. This would also increase the knowledge on the accuracy of the method for generating the tracers. Moreover, for a complete overview, it is important to study not only the surface velocities but the velocities over the entire depth of the stream.

Lastly, it is recommended to manage a more strict definition of flow separation zones, such that small separation zones would be excluded. For example, flow separation zones smaller than 1/8 of the width, as done by Parsons (2003).

This research has shown that flow separation zones can occupy a large area of the flow within natural, meandering streams. It should be noted that the size of these separation zones can differ significantly per bend, ranging from no separation zones to large separation zones covering almost the entire width of the surface flow. Controlling factors found in literature, often based on idealized laboratory or numerical studies, are not directly applicable to natural streams and thus the factors controlling the onset and size of these flow separation zones remain not entirely clear. It is recommended to use this research as a lead to further research the occurrence of flow separation zones. When it is intended to include flow separation in hydrodynamic models, this study shows that further research in natural streams is required to adequately determine the controlling factors of flow separation. In renaturalization projects, flow separation zones should be taken into account, as this study shows that the presence or absence of flow separation zones can significantly influence the effective width of meandering streams.

6 Conclusions

In this study, ten river bends in the Glanerbeek were analyzed with LSPIV to observe the surface flow patterns. The field study was executed in a naturally formed meandering stream and provides a thorough comparison with laboratory and numerical studies. In this chapter, the answer to the sub-questions will be given, with which eventually the main question will be answered.

How does the surface flow pattern in the bends differ with varying water levels?
The surface flow pattern has been observed for two different water levels. On the day with the highest water level (day 1), the maximum velocities throughout the river bends are approximately 0.1 m/s higher than on the day with the lower water level (day 3). It was found that both the inner and the outer bend separation zones were larger with lower water levels. This difference was largest for the inner bend separation zones. Moreover, topographic steering was more prevalent for lower flow depths, which could have resulted in the larger inner bend flow separation zone during the third measurement day.

Which characteristics correlate with the size of the flow separation zones?
The correlation between the four characteristics of the river bend and the size of the separation zones has been analysed. These characteristics were the R/B ratio, the radius, the impingement angle and the increase in cross-sectional area. The largest correlation was found for the increase in cross-sectional area and the outer bend separation zone. This correlation was of comparable magnitude on both measurement days. The correlation is negative, meaning the the size of the separation zone decreases for an increase in cross-sectional area, which is contrary to the literature and can most likely be attributed to the assumption that the increase in cross-sectional area is the largest around the apex.

Next, there is a negative correlation between the impingement angle and the outer bend separation zone. This relation is more prevalent on the first measurement day, so with a higher water depth. The correlation between the radius and the outer bend separation zone is also negative, which means that the size of the outer bend separation increases with increasing curvature.

The last parameter is the only parameter that correlates with the inner bend separation zone. The R/B ratio shows a negative correlation with the inner bend separation zone. This correlation is more pronounced on the first measurement day, with higher water depths.

The lack of correlation between the other parameters can be caused by multiple factors. The focus is now solely on a linear relation, so there could be a non-linear correlation. In some cases, the lack of correlation could be caused by the methodology used. The sample size is small, which can result in a large attribution of outliers, influencing the correlation coefficient.

What are the differences between inner and outer bend separation zones and their geometric and flow characteristics?
The main difference found between the inner and outer bend separation zones is that the inner bend separation zone occurs more often than the outer bend separation zone. Moreover, the size of the inner bend separation zones is slightly larger compared to the outer bend separation zones. In both separation zones, the flow was stagnant in almost all bends, and almost no recirculation zones were observed.

How do these results correspond to controlling factors of flow separation observed in other rivers?
In the section below, the result of each possible potential controlling factor of flow separation is compared to findings in literature. Also, the difference between inner and outer bend separation will be discussed. The comparison is made with laboratory, numerical modelling and field studies. It should be noted that most studies identifying controlling factors are laboratory or numerical studies, which can identify possible controlling factors more easily due to the idealized setting of the study.

- Water level

  In literature, the overall consensus is that the size of flow separation increases with increasing water depth (Bo and Ralston, 2020; Blanckaert et al., 2013). However, some studies found that the water depth did not influence the size of the flow separation zone (Kleinhans et al., 2010) or that the size of the inner bend separation zone increases with decreasing flow depth (Kasvi et al., 2013). In this study, it was found that the size of flow separation zones negatively correlated with the water depth. The increase in size of flow separation areas with decreasing water depth is strongest for the inner bend separation zone.

- Radius

  According to literature outer bend flow separation is larger for smaller radii (Kim et al., 2020). In this study, it was found that the flow separation is indeed negatively correlated with the radius and is in agreement with the literature. No relation was found between the size of the outer bend flow separation zone and the radius of the river bend.

- R/B ratio

  In literature, flow separation is expected to occur at a $R/B < 2$ (Bagnold, 1960; Finotello et al., 2020; Nanson, 2010) or $R/B < 3$ (Bagnold, 1960; Hickin and Nanson, 1975). In this study, the relation with the R/B ratio was found to be negatively correlated with the size of the inner bend separation zones. The R/B ratios found ranged from 2.1 to 4.8. Inner bend separation zones were present for each of these R/B ratios. Therefore, the negative correlation between the R/B ratio and the size of the flow separation zones is in agreement with the literature, but the onset of flow separation from a specific value of R/B is not. It is reasonable that a specific value for the onset of flow separation can be detected in idealized laboratory and numerical studies, but it is reasonable that such a specific threshold cannot be identified in a field study.

- Impingement angle

  The relation with the impingement angle was mainly found by Parsons (2003), although the importance of the inflow conditions was also emphasized by other studies (e.g. Ferguson et al., 2003; Hodskinson and Ferguson, 1998 and Nanson, 2010). In this study, a negative correlation was found between the impingement angle and the outer bend separation zone, while Parsons (2003) found a positive correlation between the impingement angle and both the inner and the outer bend separation zones. Hence, This study shows the significance of the impingement angle. However, the relation is contrary to Parsons (2003).

- Increase in cross-sectional area

  The increase in cross-sectional area was studied by Blanckaert et al. (2013) and Vermeulen et al. (2015). They found that a significant increase in cross-sectional area results in an increase in the onset and size of flow separation at both banks. However, in this study, it was found that the increase in cross-sectional area only correlates with the outer bend flow separation zones. Moreover, the relation found in this study was negative, resulting in a decrease in flow separation area with an increase in cross-sectional area.

- Difference between inner and outer bend separation

  In literature, it was found that the inner bend flow separation occurs more often than outer bend flow separation (Blanckaert, 2010; Hooke, 2013; Parsons, 2003). Parsons (2003) found that the size of the outer bend separation zones is usually larger. In this study, the inner bend separation area was more prevalent and the average size of the separation zones was larger for these inner bend separation zones. In inner bend separation zones, recirculation is often observed in literature (Blanckaert, 2010; Blanckaert et al., 2013; Kasvi et al., 2013). However, in this study, all inner bend separation zones showed stagnant flow and no recirculating pattern. In the outer bend, a recirculating flow was found at one bend on one measurement day.

With the use of the answers to the sub-questions, the main research question can be answered:

Which geometric and flow characteristics are controlling factors for the onset and size of flow separation in the Glanerbeek?

The factors influencing the occurrence and size of the flow separation zones in the Glanerbeek are the water depth, radius, R/B ratio, impingement angle and increase in cross-sectional area, of which an overview can be found in Table 13. The impingement angle and the increase in cross-sectional area showed the highest correlation. A decrease in water depth correlated with an increase in the size of the flow separation zones, at both the inner and the outer bend. The R/B ratio correlated solely with the size of the inner bend separation zones, which increased with a decreasing R/B ratio. The radius, impingement angle and increase in cross-sectional area correlated with the outer bend separation, such that an increase in these parameters leads to a decrease in the size of the flow separation zones. It should be noted that these factors are correlating factors and cannot be seen as characteristics causing flow separation. Additionally, no specific threshold values have been found that induce the onset of flow separation zones.

Table 13: Overview of whether a correlation was found between the inner and/or outer bend with the parameters. A + sign denotes a positive correlation, - a negative correlation and when no value is present, no correlation was found

Parameter:	Inner bend flow separation area	Outer bend flow separation area
Flow depth	-	
Radius		-
R/B	-	
Impingement angle		-
Increase in cross-sectional area		-

References

Bagnold, R. A. (1960). *Some Aspects of the Shape of River Meanders*. US Government Printing Office.

Blanckaert, K. (2010). Topographic steering, flow recirculation, velocity redistribution, and bed topography in sharp meander bends. *Water Resources Research*, *46*(9), 2095–2170.

Blanckaert, K. (2015). Flow separation at convex banks in open channels. *Journal of Fluid Mechanics*, *779*, 432–467.

Blanckaert, K. (2018). Hydro-sedimentological processes in meandering rivers: A review and some future research directions. *Fluvial Meanders and Their Sedimentary Products in the Rock Record*, 297–319.

Blanckaert, K., & De Vriend, H. J. (2010). Meander dynamics: A nonlinear model without curvature restrictions for flow in open-channel bends. *Journal of Geophysical Research: Earth Surface*, *115*(F4).

Blanckaert, K., Kleinhans, M. G., McLelland, S. J., Uijttewaal, W. S., Murphy, B. J., Van de Kruijs, A., Parsons, D. R., & Chen, Q. (2013). Flow separation at the inner (convex) and outer (concave) banks of constant-width and widening open-channel bends. *Earth Surface Processes and Landforms*, *38*(7), 696–716.

Bo, T., & Ralston, D. K. (2020). Flow Separation and Increased Drag Coefficient in Estuarine Channels With Curvature. *Journal of Geophysical Research: Oceans*, *125*(10), 1–25.

Bradley, A. A., Kruger, A., Meselhe, E. A., & Muste, M. V. (2002). Flow measurement in streams using video imagery. *Water Resources Research*, *38*(12), 51–1.

Creëlle, S., Roldan, R., Herremans, A., Meire, D., Buis, K., Meire, P., Van Oyen, T., De Mulder, T., & Troch, P. (2018). Validation of large-scale particle image velocimetry to acquire free-surface flow fields in vegetated rivers. *Journal of Applied Water Engineering and Research*, *6*(3), 171–182.

Dal Sasso, S., Pizarro, A., Samela, C., Mita, L., & Manfreda, S. (2018). Exploring the optimal experimental setup for surface flow velocity measurements using PTV. *Environmental monitoring and assessment*, *190*, 1–14.

Dal Sasso, S., Pizarro, A., & Manfreda, S. (2020). Metrics for the quantification of seeding characteristics to enhance image velocimetry performance in rivers. *Remote Sensing*, *12*(11), 1789.

Detert, M. (2021). How to avoid and correct biased riverine surface image velocimetry. *Water Resources Research*, *57*(2), e2020WR027833.

Dramais, G., Le Coz, J., Camenen, B., & Hauet, A. (2011). Advantages of a mobile LSPIV method for measuring flood discharges and improving stage–discharge curves. *Journal of Hydro-Environment Research*, *5*(4), 301–312.

Engel, F. L., & Rhoads, B. L. (2012). Interaction among mean flow, turbulence, bed morphology, bank failures and channel planform in an evolving compound meander loop. *Geomorphology*, *163*, 70–83.

Ferguson, R. I., Parsons, D. R., Lane, S. N., & Hardy, R. J. (2003). Flow in meander bends with recirculation at the inner bank. *Water Resources Research*, *39*(11), 1322.

Finotello, A., Ghinassi, M., Carniello, L., Belluco, E., Pivato, M., Tommasini, L., & D'Alpaos, A. (2020). Three-Dimensional Flow Structures and Morphodynamic Evolution of Microtidal Meandering Channels. *Water Resources Research*, *56*(7), e2020WR027822.

Fox, R., McDonald, A., Pritchard, P., & Mitchell, J. (2016). *Fluid mechanics* (9th edition). Wiley.

Furbish, D. J. (1991). Spatial autoregressive structure in meander evolution. *Geological Society of America Bulletin*, *103*(12), 1576–1589.

Geertsema, T. J., Torfs, P. J., Eekhout, J. P., Teuling, A. J., & Hoitink, A. J. (2020). Wood-induced backwater effects in lowland streams. *River Research and Applications*, *36*(7), 1171–1182.

Hasenbos, C. (n.d.). *Rivier de Dinkel van boven*. https://www.werkaandemuur.nl/nl/werk/Rivier-de-Dinkel-van-boven/381680

Hickin, E. J., & Nanson, G. C. (1975). The character of channel migration on the Beatton River, northeast British Columbia, Canada. *Geological Society of America Bulletin*, *86*(4), 487–494.

Hodskinson, A., & Ferguson, R. (1998). Numerical modelling of separated flow in river bends: Model testing and experimental investigation of geometric controls on the extent of flow separation at the concave bank. *Hydrological Processes*, *12*(8), 1323–1338.

Hooke, J. (2013). River meandering. In E. Wohl (Ed.), *Treatise on geomorphology* (pp. 260–288). Academic Press San Diego, Calif.

Jon. (2024). RivMAP - River Morphodynamics from Analysis of Planforms [MATLAB Central File Exchange. Retrieved June 5, 2024].

Kasvi, E. (2015). *Fluvio-morphological processes of meander bends-combining conventional field measurements, close-range remote sensing and computational modelling* [Doctoral dissertation, University of Turku].

Kasvi, E., Vaaja, M., Alho, P., Hyyppä, H., Hyyppä, J., Kaartinen, H., & Kukko, A. (2013). Morphological changes on meander point bars associated with flow structure at different discharges. *Earth Surface Processes and Landforms*, *38*(6), 577–590.

Kim, J. S., Seo, I. W., Baek, D., & Kang, P. K. (2020). Recirculating flow-induced anomalous transport in meandering open-channel flows. *Advances in Water Resources*, *141*, 103603.

Kim, Y.-G., Roh, Y.-S., & Yoon, B.-M. (2004). Verification and application of surface-velocity measurement method using LSPIV. *Journal of Korea Water Resources Association*, *37*(2), 155–161.

Kim, Y. (2006). *Uncertainty analysis for non-intrusive measurement of river discharge using image velocimetry*. The University of Iowa.

Kleinhans, M. G., Blanckaert, K., Mc Lelland, S. J., Uijttewaal, W. S., Murphy, B. J., van de Kruijs, A., & Parsons, D. (2010). Flow separation in sharp meander bends. *Proceedings of the HYDRALAB III Joint User Meeting*, (CONF).

Koninklijk Nederlands Meteorologisch Instituut. (2024a). Achtergrond: Daggegevens van het weer [Accessed on June 3, 2024].

Koninklijk Nederlands Meteorologisch Instituut. (2024b). Daggegevens van het weer in nederland [Accessed on June 3, 2024].

Legleiter, C. J., & Kinzel, P. J. (2020). Inferring surface flow velocities in sediment-laden Alaskan rivers from optical image sequences acquired from a helicopter. *Remote Sensing*, *12*(8), 1282.

Lewis, Q. W., & Rhoads, B. L. (2018). LSPIV measurements of two-dimensional flow structure in streams using small unmanned aerial systems: 1. accuracy assessment based on comparison with stationary camera platforms and in-stream velocity measurements. *Water Resources Research*, *54*(10), 8000–8018.

Liu, W.-C., Lu, C.-H., & Huang, W.-C. (2021). Large-scale particle image velocimetry to measure streamflow from videos recorded from unmanned aerial vehicle and fixed imaging system. *Remote Sensing*, *13*(14), 2661.

MathWorks. (2021a). *Computer vision toolbox* [Version 9.3 (R2021a)]. MathWorks. Natick, Massachusetts.

MathWorks. (2021b). *Image processing toolbox* [Version 11.3 (R2021a)]. MathWorks. Natick, Massachusetts.

Merritt, D. M., & Wohl, E. E. (2002). Processes governing hydrochory along rivers: Hydraulics, hydrology, and dispersal phenology. *Ecological applications*, *12*(4), 1071–1087.

Meselhe, E., Peeva, T., & Muste, M. (2004). Large scale particle image velocimetry for low velocity and shallow water flows. *Journal of Hydraulic Engineering*, *130*(9), 937–940.

Muste, M. (2004). Flow diagnostic in hydraulic modeling using image velocimetry. *J. Hydraul. Eng.*, *130*(3), 175–185.

Muste, M., Fujita, I., & Hauet, A. (2008). Large-scale particle image velocimetry for measurements in riverine environments. *Water resources research*, *44*(4).

Nanson, R. A. (2010). Flow fields in tightly curving meander bends of low width-depth ratio. *Earth Surface Processes and Landforms: The Journal of the British Geomorphological Research Group*, *35*(2), 119–135.

Newcastle University. (2024). Strength of correlation [Accessed: 2024-06-19].

Parsons, D. R. (2003). *Flow separation in meander bends.* [Doctoral dissertation, University of Sheffield].

Pearce, S., Ljubicic, R., Peña-Haro, S., Perks, M., Tauro, F., Pizarro, A., Dal Sasso, S. F., Strelnikova, D., Grimaldi, S., Maddock, I., Paulus, G., Plavsic, J., Prodanovic, Dusan, & Manfreda, S. (2020). An Evaluation of Image Velocimetry Techniques under Low Flow Conditions and High Seeding Densities Using Unmanned Aerial Systems. *Remote Sensing*, *12*(2), 232.

Pizarro, A., Dal Sasso, S., & Manfreda, S. (2020a). Refining image-velocimetry performances for streamflow monitoring: Seeding metrics to errors minimization. *Hydrological Processes*, *34*(25), 5167–5175.

Pizarro, A., Dal Sasso, S. F., Perks, M., & Manfreda, S. (2020b). Spatial distribution of tracers for optical sensing of stream surface flow. *Hydrology and Earth System Sciences Discussions*, *24*(11), 1–19.

Provincie Overijssel. (2021). Factsheet: Glanerbeek.

Pumo, D., Alongi, F., Ciraolo, G., & Noto, L. V. (2021). Optical Methods for River Monitoring: A Simulation-Based Approach to Explore Optimal Experimental Setup for LSPIV. *Water*, *13*(3), 247.

Ran, Q.-h., Li, W., Liao, Q., Tang, H.-l., & Wang, M.-y. (2016). Application of an automated LSPIV system in a mountainous stream for continuous flood flow measurements. *Hydrological Processes*, *30*(17), 3014–3029.

Sharif, O. (2022). *Measuring surface water flow velocities by a drone and large-scale partice image velocimetry (LSPIV)* [Master's thesis, University of Twente].

Takasu, T., & Yasuda, A. (2009). Development of the low-cost RTK-GPS receiver with an open source program package RTKLIB. *International symposium on GPS/GNSS*, *1*, 1–6.

Tauro, F., Petroselli, A., & Grimaldi, S. (2018). Optical sensing for stream flow observations: A review. *Journal of Agricultural Engineering*, *49*(4), 199–206.

Tauro, F., Piscopia, R., & Grimaldi, S. (2017). Streamflow observations from cameras: Large-scale particle image velocimetry or particle tracking velocimetry? *Water Resources Research*, *53*(12), 10374–10394.

Thielicke, W., & Sonntag, R. (2021). Particle image velocimetry for matlab: Accuracy and enhanced algorithms in pivlab. *Journal of Open Research Software*, *9*(1).

Thielicke, W., & Stamhuis, E. J. (2014). PIVlab – towards user-friendly, affordable and accurate digital particle image velocimetry in matlab. *Journal of Open Research Software*. https://doi.org/10.5334/jors.bl

Venditti, J. G., Rennie, C. D., Bomhof, J., Bradley, R. W., Little, M., & Church, M. (2014). Flow in bedrock canyons. *Nature*, *513*(7519), 534–537.

Vermeulen, B., Hoitink, A., & Labeur, R. (2015). Flow structure caused by a local cross-sectional area increase and curvature in a sharp river bend. *Journal of Geophysical Research: Earth Surface*, *120*(9), 1771–1783.

Waterschap Vechtstromen. (2019, November). Projectplan Waterwet Glanerbeek Klooster - N35 [Accessed: 2024-06-19].

Waterschap Vechtstromen. (n.d.). *Glanerbeek*. Retrieved May 29, 2024, from https://www.vechtstromen.nl/projecten/actuele-projecten/dinkeldal/glanerbeek/

Waterschap Vechtstromen. (2021-2024). Glanerbeek Mullermansbrug [Dataset received personally from Duineveld, M. on April 11, 2024].

Appendix

A Area of flow separation per measurement day

Table 14: Area of inner- and outer bend flow separation per bend for three different water heights

	Inner bend separation area $[m^2]$		Outer bend separation area $[m^2]$	
Water height [+NAP]	33.39 (day 1)	33.10 (day 3)	33.39 (day 1)	33.10 (day 3)
Bend 1	18.2 - 49.0	26.7 - 32.9	27.2	6.0 - 34.6
Bend 2	0 - 0.9	17.9 - 31.1	17.8 - 20.3	31.9 - 40.4
Bend 3	7.8 - 20.1	30.9 - 35.6	15.2 - 37.6	30.9 - 38.8
Bend 4	33.9 - 63.0	29.5	22.8 - 24.6	19.4 - 22.8
Bend 5	27.2 - 45.8	25.5 - 32.2	0	0 - 4.3
Bend 6	21.2 - 34.2	28.0 - 35.3	2.9 - 8.2	3.4 - 16.0
Bend 7	4.3 - 10.9	21.2 - 24.5	0 - 1.7	0
Bend 8	2.5 - 9.0	9.3 - 19.1	5.0 - 7.8	3.2
Bend 9	16.2 - 29.9	22.6 - 25.2	0	0
Bend 10	3.3 - 13.7	16.0 - 18.6	0 - 2.1	0

B Bend characteristics

Table 15: Bend characteristics

Bend characteristics	**Bend 1**			**Bend 2**			**Bend 3**			**Bend 4**			**Bend 5**		
Radius [m]	7.3			29.9			29.3			22.6			35.8		
R/B	2.3			4.5			3.9			2.9			4.6		
Cross-sectional area [m^2]	2.9	4.1	2.9	2.9	3.1	2.7	2.7	1.8	2.2	2.2	1.5	1.2	1.2	2.0	1.5
Impingement angle [°]	15			35			10			45			45		

Bend characteristics	**Bend 6**			**Bend 7**			**Bend 8**			**Bend 9**			**Bend 10**		
Radius [m]	21.7			27.0			36.1			16.0			22.8		
R/B	2.7			4.3			4.8			2.1			3.3		
Cross-sectional area [m^2]	1.0	1.7	1.1	1.2	1.9	2.5	2.5	2.0	1.4	1.4	2.7	1.2	1.2	1.2	1.4
Impingement angle [°]	40			35			20			40			40		

C Results on day 2

Table 16: Area of inner- and outer bend flow separation per bend for three different water heights

	Inner bend separation area $[m^2]$			Outer bend separation area $[m^2]$		
Water height [+NAP]	33.39 (day 1)	33.20 (day 2)	33.10 (day 3)	33.39 (day 1)	33.20 (day 2)	33.10 (day 3)
Bend 1	18.2 - 49.0	40.5 - 42.9	26.7 - 32.9	27.2	18.3 - 35.0	6.0 - 34.6
Bend 2	0 - 0.9	21.3 - 42.7	17.9 - 31.1	17.8 - 20.3	17.4 - 18.8	31.9 - 40.4
Bend 3	7.8 - 20.1	36.1 - 43.7	30.9 - 35.6	15.2 - 37.6	8.5 - 18.9	30.9 - 38.8
Bend 4	33.9 - 63.0	11.1 - 18.1	29.5	22.8 - 24.6	15.8 - 16.7	19.4 - 22.8
Bend 5	27.2 - 45.8	9.7 - 13.3	25.5 - 32.2	0	0 - 1.4	0 - 4.3
Bend 6	21.2 - 34.2	14.0 - 21.5	28.0 - 35.3	2.9 - 8.2	0	3.4 - 16.0
Bend 7	4.3 - 10.9	23.4 - 24.4	21.2 - 24.5	0 - 1.7	0	0
Bend 8	2.5 - 9.0	14.5 - 18.0	9.3 - 19.1	5.0 - 7.8	1.3 - 2.3	3.2
Bend 9	16.2 - 29.9	6.5 - 8.6	22.6 - 25.2	0	9.7 - 17.4	0
Bend 10	3.3 - 13.7	7.7 - 8.9	16.0 - 18.6	0 - 2.1	0	0